

**ECONOMIC GEOLOGY
RESEARCH UNIT**

University of the Witwatersrand
Johannesburg

**FLUID CHARACTERISTICS OF GRANITOID-HOSTED
GOLD DEPOSITS IN THE BIRIMIAN
TERRANE OF GHANA :
A FLUID INCLUSION MICROTHERMOMETRIC
AND RAMAN SPECTROSCOPIC STUDY**

Y. YAO, P. J. MURPHY AND L. J. ROBB

• **INFORMATION CIRCULAR No. 336**

**UNIVERSITY OF THE WITWATERSRAND
JOHANNESBURG**

**FLUID CHARACTERISTICS OF GRANITOID-HOSTED GOLD
DEPOSITS IN THE BIRIMIAN TERRANE OF GHANA: A FLUID
INCLUSION MICROThERMOMETRIC AND RAMAN
SPECTROSCOPIC STUDY**

by

Y. YAO¹, P. J. MURPHY², AND L. J. ROBB¹

(1: Department of Geology, University of the Witwatersrand, P/Bag 3, WITS 2050, South Africa
2: Raman - Luminescence Laboratory and Economic Geology Research Unit, University of the Witwatersrand,
Private Bag 3, WITS 2050, Johannesburg, South Africa)

**ECONOMIC GEOLOGY RESEARCH UNIT
INFORMATION CIRCULAR No. 336**

September, 1999

FLUID CHARACTERISTICS OF GRANITOID-HOSTED GOLD DEPOSITS IN THE BIRIMIAN TERRANE OF GHANA: A FLUID INCLUSION MICROTHERMOMETRIC AND RAMAN SPECTROSCOPIC STUDY

ABSTRACT

Fluid inclusions in vein quartz from 10 granitoid-hosted gold deposits and prospects in the Birimian terrane of Ghana, as well as from the Sansu mine (Ashanti shear zone type) and quartz veins in the non-mineralized Princess Town granodiorite, were studied by microthermometry and Raman microspectrometry. Fluid inclusions from the granitoid-hosted gold deposits are dominated by aqueous $H_2O-CO_2\pm NaCl$ and gaseous $CO_2-N_2\pm CH_4$ types, with minor (<10%) aqueous $H_2O\pm NaCl$ types. In most cases, these fluid inclusions co-exist in individual samples and show various CO_2 phase volume proportions at 25 °C. Co-existing H_2O -rich liquid and CO_2 -rich vapor fluid inclusions homogenized into liquid and carbonic vapor phases, respectively, over the same temperature range ($T_h(L)$: commonly 200 to 350 °C; $T_h(V)$: typically 210 to 350 °C). The petrographic observations and microthermometric data suggest that the fluid inclusions were trapped during phase separation of an originally homogeneous H_2O-CO_2 liquid, with low salinity (<6 wt.% NaCl equivalent) and moderate to high density (0.65 to 0.95 g/cm³). Trapping temperatures and pressures, estimated from fluid inclusion microthermometry and isochores, cluster between 200 and 350 °C, and 0.3 and 3 kbar. These values coincide with mesothermal *P-T* conditions estimated from alteration mineral assemblages. By contrast, fluid inclusions in the Sansu mine at Ashanti mainly comprise gaseous $CO_2-N_2\pm CH_4$ types. These inclusions are considered to represent post-entrapment modifications of trapped fluids. In addition, fluid inclusions in barren vein quartz from the Princess Town granodiorite comprise low salinity (commonly <6 wt.% NaCl equivalent) $H_2O\pm NaCl$ types. Raman microspectrometry shows that gaseous components of fluid inclusions from both granitoid- and shear zone-hosted gold deposits are mainly composed of CO_2 (80 to 95 mol%), with significant amounts of N_2 (2 to 20 mol%) and CH_4 (0 to 10 mol%).

The distinct low-salinity H_2O-CO_2 -rich fluids from the granitoid-hosted gold deposits are comparable in composition to those from the major Ashanti and Tarkwaian types of gold deposits in the Birimian terrane of Ghana. These fluids are most likely to be metamorphic in origin and associated with a late stage of the regional Birimian orogeny; there is little or no evidence of a magmatic fluid component in the granitoid-hosted gold deposits. Gold deposition in the Birimian granitoids was related to fluid phase separation and sulphidization of host rocks during hydrothermal alteration and mineralization. The granitoids are considered to have acted as preferential sites for fluid flow and ore precipitation due to their brittle nature during regional deformation. The present study, together with previous publications, suggests that fluid inclusions are characterized by $H_2O-CO_2\pm NaCl$ and/or $CO_2-N_2\pm CH_4$ types in mineralized areas, whereas $H_2O\pm NaCl$ fluid compositions dominate in barren areas. Fluid inclusion characteristics may, therefore, be a useful tool for regional gold exploration in the Birimian terrane of Ghana.

— oOo —

FLUID CHARACTERISTICS OF GRANITOID-HOSTED GOLD DEPOSITS IN THE BIRIMIAN TERRANE OF GHANA: A FLUID INCLUSION MICROTHERMOMETRIC AND RAMAN SPECTROSCOPIC STUDY

CONTENTS

	Page
INTRODUCTION	1
METHODOLOGY	2
BIRIMIAN GRANITOIDS AND THEIR ASSOCIATED GOLD DEPOSITS	3
FLUID INCLUSIONS	6
Petrography	6
Fluid inclusion types	6
Microthermometric data	11
Raman microspectrometric results	23
DISCUSSION	24
Fluid immiscibility	24
P-T conditions of mineralization	25
Oxygen fugacity ($f\text{O}_2$) of ore-forming fluids	28
Comparison of granitoid-hosted gold deposits with the Ashanti and Tarkwaian types	29
Sources of ore-forming fluids	32
Metamorphism and gold mineralization	32
CONCLUSIONS	33
ACKNOWLEDGEMENTS	34
REFERENCES	34

— oOo —

Published by the Economic Geology Research Unit
Department of Geology
University of the Witwatersrand
1 Jan Smuts Avenue
Johannesburg 2001
South Africa

ISBN 1-86838-262-1

FLUID CHARACTERISTICS OF GRANITOID-HOSTED GOLD DEPOSITS IN THE BIRIMIAN TERRANE OF GHANA: A FLUID INCLUSION MICROTHERMOMETRIC AND RAMAN SPECTROSCOPIC STUDY

INTRODUCTION

The best-known and most productive gold deposits in the Birimian terrane of Ghana are represented by the Ashanti shear zone- and Tarkwaian quartz-pebble conglomerate-types. The Ashanti-type shear-zone-hosted deposits have a total gold inventory of some 1100 tons (Milési et al., 1991), whereas the Tarkwaian conglomerate-hosted deposits have gold reserves of around 550 tons (Milesi et al., 1991; Gold Fields Ghana Ltd., personal commun., 1997). A third type of gold deposit, increasingly receiving the attention of exploration in the region, are the granitoid-hosted gold deposits, which contain estimated gold reserves/resources of over 100 tons at an average grade of 2 to 4 g/t (Ashanti Goldfields Co., Mutual Ghana Ltd., Takoradi Gold N.L., personal commun., 1997). The present study focuses on these granitoid-hosted gold deposits and describes the nature of fluids associated with mineralization and their relationships to the other major gold deposit types in the region.

The Palaeoproterozoic (Birimian) geology of Ghana is defined by five relatively evenly spaced NE-SW-striking volcanic belts, separated by intervening sedimentary basins (Fig. 1). Volcanic and sedimentary rocks are thought to be coeval with the sediments representing lateral facies equivalents of the volcanic belts (Leube and Hirdes, 1986; Leube et al., 1990); these successions formed at about 2.0 to 2.2 Ga (Hirdes et al., 1992; Taylor et al., 1992; Oberthür et al., 1998). The volcanic belts are composed mainly of deformed basaltic meta-lavas, intruded by coeval tonalitic to granitic plutons, which are in turn overlain in certain of the belts by Tarkwaian sedimentary rocks (conglomerates, sandstones and slates) deposited between 2095 ± 10 and 2132 ± 3 Ma (Hirdes and Nunoo, 1994). The intervening sedimentary basins (volcaniclastics, wackes, argillites) formed between 2135 ± 5 and 2184 ± 3 Ma (Davis et al., 1994) and are also intruded by areally extensive granitoids. Regional deformation and metamorphism are related to the Eburnean tectonothermal event at about 2100 Ma (Eisenlohr and Hirdes, 1992; Oberthür et al., 1998). The metamorphic grade of Birimian rocks is commonly of greenschist facies, but locally reaches the epidote-amphibolite and amphibolite facies, especially in parts of the Ashanti and Kibi Winneba belts (Klemd, 1998).

The Ashanti-type gold deposits occur in strongly folded and sheared volcanic rocks, mainly along the western margins of the Ashanti belt, and comprise quartz-sulphide (mainly arsenopyrite) veins in steeply dipping shear zones, as well as disseminated sulphides (mainly pyrite) in the metavolcanic rocks. These gold deposits are suggested to be syn-metamorphic (Oberthür et al., 1994). Tarkwa-type conglomerate-hosted gold deposits mainly occur in the southern parts of the Ashanti belt and are considered to be syngenetic palaeo-placers considerably modified by input of later fluids which have pervasively altered the original mineral assemblage (Klemd et al., 1993; Hirdes and Nunoo, 1994).

Fluid inclusions from both the Ashanti and Tarkwaian types of gold deposits are dominated by gaseous high-density (up to 1.1 g/cm^3) $\text{CO}_2\text{-N}_2\pm\text{CH}_4$ compositions, with minor aqueous $\text{H}_2\text{O}\text{-CO}_2\pm\text{NaCl}$ and $\text{H}_2\text{O}\pm\text{NaCl}$ bearing fluid inclusions, of low salinities (generally <6 wt.% NaCl equivalent; Schwartz et al., 1992; Oberthür et al., 1994; Klemd et al., 1993, Schmidt Mumm et al., 1997). The origin of these fluids is currently a topic of debate. Schmidt Mumm et al. (1997, 1998) argued that mineralizing fluids in the Ashanti belt were derived from a CO_2 -rich, nearly H_2O -free hydrothermal system. By contrast, Schwartz et al. (1992), Klemd

and Hirdes (1997), and Klemd (1998) suggested that gaseous CO₂-rich and aqueous H₂O-rich fluid inclusions resulted from fluid immiscibility and/or grain-boundary migration/recrystallization during the ductile-brittle deformation of the Birimian terrane. Schmidt Mumm et al. (1997) also reported that primary fluid inclusions in vein quartz from the Ayansuri granite-hosted gold deposit mainly comprise gaseous CO₂-rich and aqueous H₂O-rich types, of low salinity (<3 wt.% NaCl equivalent). These fluids were suggested to have been trapped during phase separation of mineralizing solutions (Schmidt Mumm et al., 1997).

This paper presents the results of a comprehensive microthermometric (>2600 measurements) and Raman spectrometric (>90 analyses) study of fluid inclusions in vein quartz from 10 major granitoid-hosted gold deposits and prospects in the Birimian terrane of Ghana. In addition, the Sansu mine from the Ashanti shear zone system and barren quartz veins from the non-mineralized Princess Town granodiorite were also studied for comparative purposes. The samples studied cover a wide area from southeast to northwest Ghana (Fig. 1). The objectives of this study are to document the regional characteristics of mineralizing fluids depositing gold in the Birimian granitoids and to construct the *P-T* conditions of entrapment of the fluids. On the basis of fluid inclusion data, as well as geological setting and geochemical characteristics of ores, an attempt is made to investigate the genetic link, if any, of ore-forming fluids among the shear zone-, conglomerate-, and granitoid-hosted gold deposits and to discuss the genesis of gold mineralization in the Birimian granitoids. The relevance of fluid inclusion characteristics as an indicator for regional gold exploration in the Birimian of Ghana is also mentioned.

METHODOLOGY

Fluid inclusion microthermometry was carried out at the University of the Witwatersrand, South Africa, using a Linkham TH 600 heating-cooling stage and an OLYMPUS VANOX microscope with an ULWD MSPlan 50x lens. The SYNFLINC synthetic standards of CO₂ and aqueous H₂O fluid inclusions were measured for calibration of the stage in this study. Most measurements were made at heating rates of 0.2 to 10 °C/min. Clathrate melting temperatures (T_{melt}) were determined by temperature cycling (Roedder, 1963; Diamond, 1990), with heating rates near T_{melt} of 0.2 to 0.5 °C/min. The reproducibility of measurements was better than ± 0.2 °C below +30 °C and ± 2 °C at total homogenization temperature, when the chips were centred in the specimen holder. Calculations of salinity, mole fractions (X_{H2O}, X_{CO2}, X_{NaCl}), density of carbonic phase and bulk fluids (ρ_{CO2}, ρ_b), and isochores of fluid inclusions were made using published equations of state: Bowers and Helgeson (1983) for H₂O-CO₂±NaCl fluid inclusions; Holloway (1981) for gaseous fluid inclusions; and Zhang and Frantz (1987) for H₂O±NaCl fluid inclusions.

Raman analyses of fluid inclusions were carried out at the University of the Witwatersrand, South Africa, using a Jobin-Yvon T64000 spectrometer in a single spectrograph mode. The 514.532 nm line of a Coherent Argon ion laser was used, with a source power of 700 mW (reduced to <100 mW at the sample surface) and a focused spot size of 1 μm. The laser was focused onto samples using an OLYMPUS BH-40 microscope and MPlan 100x lens. Spectra were acquired using a liquid nitrogen-cooled Spectrum One CCD detector with a pixel size of 27 μm (1024x256 pixels). Integration time was generally 150s for each range (with 2 accumulations averaged and cosmic rays rejected). Data manipulation was carried out using the Jobin-Yvon/Spex SpectraMax software and peak areas calculated using peak-fitting routines in the Microcal Origin program. Where nitrogen was detected, an analysis under identical conditions was carried out in quartz near the inclusion, at the same focal depth, to test for contamination by atmospheric nitrogen. When atmospheric nitrogen was detected

the appropriate peak area was subtracted from the nitrogen peak for the inclusion, and this usually represented no more than 1 or 2 wt% N₂. The instrumental response for CO₂ and N₂ was tested using gas standards supplied by A. M. van den Kerkhof. No instrumental correction factor was found to be necessary, and the reproducibility was measured as \pm 5 mol% N₂ at low N₂ concentrations, and \pm 1.5 mol% N₂ at higher N₂ concentrations. Detection limits for gases in the carbonic phase of fluid inclusions in the present study were typically around 1 mol%.

The Raman analyses were conducted to obtain quantitative gaseous compositions of primary fluid inclusions. Gaseous molar volumes of fluid inclusions (MVg) were estimated by interpolation and/or extrapolation in the T_m-T_b-contoured VX diagrams of Thiéry et al. (1994). As discussed by Hall and Bodnar (1990), melting temperatures of carbonic phases (T_m) for gaseous fluid inclusions are insensitive to the vapor density. Thus, T_b and not the T_m was used to estimate gaseous molar volumes, in combination with Raman analytical results of the corresponding fluid inclusions.

BIRIMIAN GRANITOIDS AND THEIR ASSOCIATED GOLD DEPOSITS

Junner (1940) divided the Palaeoproterozoic Birimian granitoids into two major types: an older granite (G1: Cape Coast type) and a younger granite (G2: Dixcove type). This classification was widely used in geological maps of Ghana. Since the 1980s, the Birimian granitoids have been re-classified into Basin- and Belt-types on the basis of their geological association (Mauer, 1986, 1990; Leube et al., 1990). From an economic point of view, both Basin and Belt types of granitoids are further divided into non-mineralized and mineralized plutons (Yao and Robb, 1998a).

Non-mineralized Belt granitoids outcrop within volcanic belts as small- and medium-sized plutonic bodies (Fig. 1), and are typically tonalitic to granodioritic in composition. The granitoids are characterized mainly by a metaluminous character, and their mafic minerals are hornblende and/or biotite. By contrast, the non-mineralized Basin granitoids were emplaced within basin sediments as large batholiths, and they are much more restricted in chemical composition, mainly comprising granodiorite and granite. These rocks dominantly show a marginally peraluminous character. Biotite is the main mafic mineral, and hornblende is rarely observed. Accessory minerals of the Basin granitoids are similar to those of the Belt granitoids and consist of epidote and titanite, with minor zircon, apatite, and opaque minerals (Yao and Robb, 1998b).

U-Pb zircon and monazite isotope dating indicates that the Belt granitoids (2136 ± 12 to 2179 ± 2 Ma) were emplaced 10 to 90 million years before the Basin granitoids (2086 ± 4 to 2125 ± 2 Ma) (Hirdes et al., 1992, 1993; Loh and Hirdes, 1996; Oberthür et al., 1998; Yao and Robb, 1999). The age differences between both granitoid types may reflect a progressive accretion of magmatic areas from the southeast to the northwest of Ghana (Hirdes et al., 1992; Yao and Robb, 1999).

On the basis of petrographic and geochemical characteristics, as well as whole-rock Rb-Sr, Sm-Nd, and Pb-Pb isotope signatures (Taylor et al., 1988, 1992), it is suggested that the Belt granitoids are I-type granites and formed by partial melting of basaltic rocks with compositional variations being controlled largely by amphibole fractionation. By contrast, the Basin granitoids are more akin to S-type granites and are considered to have been generated by “minimum” melting of crustal materials with addition of a minor mantle component (Yao and Robb, 1998b; and references therein).

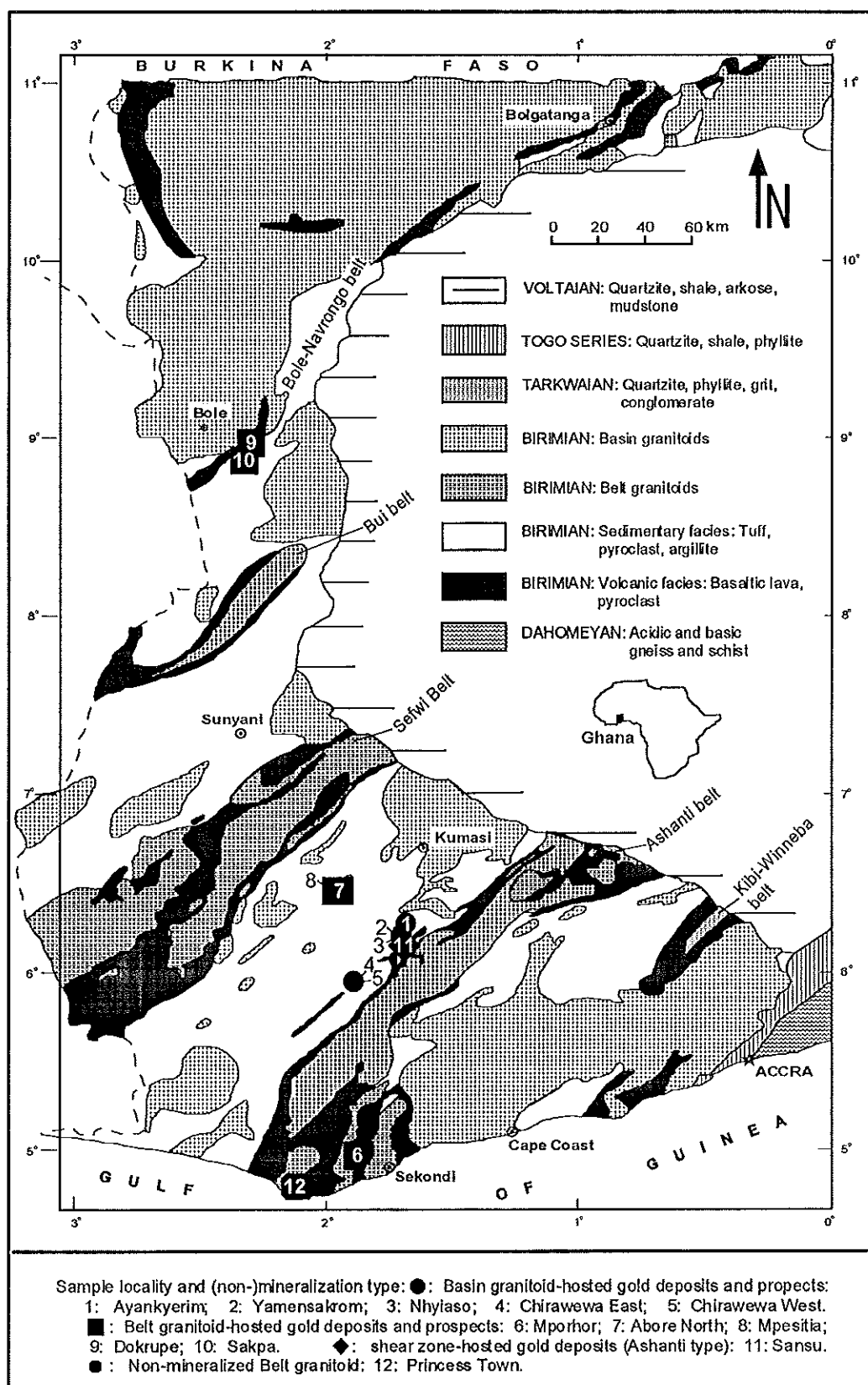


Figure 1. Simplified geological map of Ghana (modified after Hirches and Leube, 1989), showing sample localities of Basin (points 1 to 5) and Belt (points 6 to 10) granitoid-hosted gold deposits and prospects in this study. Also shown are the Sansu gold deposit at Ashanti (point 11), and barren quartz veins from non-mineralized Belt granitoid at Princess Town (point 12).

Over 20 granitoids from both Belt and Basin types are now known to host gold mineralization (Yao and Robb, 1998a). Granitoids now represent a significant new target for regional gold exploration in the Birimian orogeny. Mineralized Belt and Basin granitoids occur as small steeply dipping intrusive stocks and are concordant with regional NE-striking faults and shear zones. These plutons exist over a wide area in southwest and west-central Ghana, but are concentrated mainly in the Ashanti, Asankrangwa, and Bole-Navrongo belts, as well as the Kumasi basin (Fig. 1). The mineralized Belt and Basin granitoids are dominantly granodioritic to granitic in composition and are comparable with their non-mineralized counterparts in terms of geological, mineralogical, geochemical, and petrogenetic characteristics. Typically, however, the mineralized granitoids occur as smaller intrusions (Yao and Robb, 1999).

Yao and Robb (1999) have shown that gold mineralization within both Belt and Basin granitoids is similar, and that no specific granitoid type in the Birimian terrane of Ghana is associated with gold mineralization. The granitoids are considered to constitute favourable sites for mineralization because they provide preferential conduits for fluid flow due to their brittle character during regional deformation. The mineralization is characterized by both quartz veins/stockworks and pervasive alteration zones within granitoids. Quartz veins and veinlets commonly fill extension-related fractures and are locally deformed. Cross-cutting relationships among the quartz veins, granitoids, and sheared wall rocks suggest that gold mineralization post-dated the granitoid emplacement and was related to relatively late brittle structures developed during the Birimian orogeny. The ore mineral assemblage in all granitoid-hosted deposits is similar and dominated by pyrite and arsenopyrite, with minor chalcopyrite, sphalerite, galena, native gold, rutile, and locally developed secondary hematite. The gold is closely associated with arsenopyrite and pyrite, and also fills in micro-fractures in quartz grains.

The alteration mineral assemblage from the various granitoid-hosted deposits is also similar and comprises quartz-sericite(muscovite)-carbonate-pyrite-arsenopyrite±chlorite±tourmaline. High temperature alteration minerals, such as K-feldspar, biotite and amphibole, were not found, suggesting that the alteration was formed in typically mesothermal *P-T* conditions of about 200 to 400 °C and 1 to 3 kbar (McCuaig and Kerrich, 1994). The similarity of sulfides between the ores and alteration zones suggests that the alteration was produced by the same mineralizing fluids. The lack of sulphates and clay minerals in the alteration zones suggests that the fluids were reduced, with near neutral pH (about 5 to 6) during the mineralization process (Mikucki and Ridley, 1993). Chemical mass balance calculations for altered versus unaltered granite samples from individual deposits demonstrate that most of the major oxides and trace elements (Rb, Sr, Ba, V, Cr, Co, Ni, Zr) were buffered by the original granitoid composition, suggesting that the alteration was developed in a rock-buffered system with respect to these components.

The U-Pb isotopic age of mineralization, derived from hydrothermal rutile, is between 2110 ± 32 and 2133 ± 21 Ma for a Belt-type granodiorite from the Sakpa mine in the Bole-Navrongo belt (U-Pb zircon intrusive age: 2137 ± 10 Ma; Yao and Robb, 1999). Mineralization in the Basin-type granitoids of the Obuasi and Ayanfuri mines of the Kumasi basin is between 2086 ± 4 and 2098 ± 7 Ma (U-Pb zircon intrusive age: 2105 ± 2 Ma; Oberthür et al., 1998). These ages are about 5 to 30 million years younger than the ages of corresponding granitoid emplacement, confirming field observations that the mineralization post-dated granitoid intrusion. The age range of mineralization overlaps with that of Basin-type granitoid emplacement and, therefore, coincides with the second of the major magmatic pulses (e.g. Basin-type granitoid intrusion) of the Birimian orogeny. Mineralization, therefore, appears to be associated with a relatively late stage of the Birimian orogeny.

FLUID INCLUSIONS

Petrography

Fluid inclusions in vein quartz from five Basin granitoids at Obuasi (Nhyiaso, Ayankyerim, Yamensakrom) and Ayanfuri (Chirawewa East, Chirawewa West) in the Kumasi basin and from five Belt granitoids at Mporhor in the Ashanti belt, at Mpesetia and Abore North in the Asankrangwa belt, and at Bole (Dokrupe, Sakpa) in the Bole-Navrongo belt (Table 1) were studied by microthermometry and Raman microspectrometry. For the purpose of comparison, fluid inclusions in vein quartz from the Sansu mine at Ashanti and in barren vein quartz from the non-mineralized Belt-type Princess Town granodiorite (Table 1) were also studied. The localities of these areas studied are shown in Figure 1. Forty six doubly polished fluid inclusion sections were examined under the microscope, of which 16 samples were selected to carry out the fluid inclusion study (Table 1).

Vein quartz within granitoids and host-rock phyllites in the studied samples forms euhedral and subehedral crystals and aggregates. Except for cross-cutting micro-fractures observed in some quartz grains, the quartz shows only rare recrystallization and weak undulose extinction, which suggests that the quartz formed in a low-stress brittle regime, as indicated by field observations. In the case of Sansu mine at Ashanti, however, quartz grains are highly orientated (Fig. 4A), but their axis directions were not determined. The quartz shows strong undulose extinction and common recrystallization, and micro-fractures cross-cutting the elongated quartz grains are well developed. These characteristics indicate that the vein quartz at Sansu was formed by multi-stage ductile and brittle deformation. The structural features of quartz optically observed in this study suggest that primary fluid inclusions from the granitoid-hosted gold deposits represent original fluid entrapment without post-entrapment modifications, whereas fluid inclusions from the Sansu mine at Ashanti have been subjected to post-entrapment modifications which are attributed to grain-boundary migration/recrystallization during ductile to brittle deformation. The latter features have also been discussed by Schwartz et al. (1992), Klemd et al. (1996), Klemd and Hirdes (1997), and Klemd (1998).

In most cases, the growth zones of quartz crystals were not clearly observed, although quartz grain boundaries are clearly recognized. Fluid inclusions that occur as isolated individuals, random groups, and planar arrays in intragranular quartz crystals were inferred to be primary, whereas fluid inclusions aligned along micro-fractures in transgranular trails were designated as secondary (Figs. 2-4). Some fluid inclusions from the granitoid-hosted gold deposits show necking-down and leakage textures at room temperature (Fig. 2G, H). Such modified fluid inclusions can be identified by careful optical observation, and their microthermometric data were not compiled into the present dataset (Tables 2, 3). There is no textural evidence for inclusion stretching at room temperature, and heating rates were kept low during total homogenization of fluid inclusions to avoid stretching of fluid inclusions (Roedder, 1984).

Fluid inclusion types

Based on the petrographic characteristics of fluid inclusions at room temperature and their microthermometric characteristics, the fluid inclusions in vein quartz from the granitoid-hosted and Ashanti-type gold deposits, as well as in barren quartz veins in the Princess Town granodiorite, can be divided into the following types (Table 2, Figs. 2-4):

Table 1. Characteristics of fluid inclusions in vein quartz from granitoid- and shear zone-hosted gold deposits and from non-mineralized granodiorite in Ghana

Deposit/prospect	Location	Host rock	Intruded/wall rock	Mineral type	Metamorphic grade	Structure style	Sample No.	Sample description	Fluid inclusion size (main) (μm)	Major type	Minor type	Measured number	Modification
A: Basin granitoids from the Kumasi basin													
Ayankyerim	Obuasi	Granodiorite	Phyllite	GT	Greenschist	Extension	GH-AR-QV-10	Quartz vein from granitoid	5-58 (10-25)	1P-a, 1P-b, 2P	1S-a, 1S-b, 2S	332	some Post-Mod.
Yamensakrom*	Obuasi	Granodiorite	Phyllite	GT	Greenschist	Extension	GH-AR-QV-14	Quartz vein from phyllite	4-42 (8-20)	1P-a, 3P	1P-b, 2P	127	
Ntijiaso	Obuasi	Tonalite/trondjemite/monzogranite	Phyllite	GT	Greenschist	Extension	GH-YM-QV-16	Quartz vein from phyllite	5-62 (8-20)	1P-a	1P-b, 2P	145	
Chirawewa East	Ayanfuri	Tonalite/trondjemite	Phyllite	GT	Greenschist	Extension, deformed	GH-NS-QV-9	Quartz vein from granitoid	3-58 (6-25)	1P-a, 1P-b, 2P	1S-a	307	
Chirawewa West	Ayanfuri	Tonalite/trondjemite	Phyllite	GT	Greenschist	Extension, deformed	GH-NS-QV-23	Quartz vein with disseminated sulfides from granitoid	4-40 (6-15)	1P-a, 1P-b, 2P	1S-a, 1S-b, 2S, 3P	312	some Post-Mod.
B: Belt granitoids from the Ashanti (AT), Asankrangwa (AS), and Bole-Navrongo (BN) belts													
Mporhor*	Mporhor (AT)	Granodiorite	Volcanics	GT	Greenschist	Extension?	GH-MP-QV-6	Quartz vein from granitoid	5-55 (8-25)	1P-a, 1P-b, 2P	1S-a, 2S	203	
Above North	Above (AS)	Diorite/granodiorite/monzogranite	Phyllite	GT	Greenschist	Extension	OA-PQ-13NO19	Quartz vein with disseminated sulfides from granitoid	5-48 (10-30)	1P-a, 3P	1P-b, 2P	25	
Mpesitia*	Mpesitia (AS)	Granodiorite	Phyllite	GT	Greenschist	Extension	OA-PQ-SNO6	Quartz vein with disseminated sulfides from granitoid	5-54 (8-20)	1P-a, 1S-a	3P, 3S	73	
Dokrue	Bole (BN)	Granodiorite	Phyllite	GT	Greenschist	Extension	GH-MT-QV-31	Quartz vein with disseminated sulfides from granitoid	5-53 (8-25)	1P-a, 1P-b	2P, 1S-a, 1S-b	162	
Sakpaka	Bole (BN)	Granodiorite	Phyllite	GT	Greenschist	Extension	GH-DU-QV-2	Quartz vein with disseminated sulfides and visible gold grains from granitoid	5-15 (8-10)	1P-a	1S-a	18	
C: Shear zone-hosted (Ashanti-type) gold deposit from the Ashanti belt													
Sansu	Ashanti	Volcanics/shear zones	ST	Greenschist	Ductile-brittle, sheared zone	VGR-QV-2	Quartz vein with disseminated sulfides from shear zones, showing lamination	4-22 (5-15)	2P	2S	96	Post-Mod.	
D: Barren quartz vein within Betti granitoid from the Ashanti belt													
Princess Town	Princess Town	Granodiorite	NG	Greenschist	Extension	VGR-QV-1	Quartz vein from granitoid	5-56 (8-25)	3P, 4P	3S	132		

Note: *=prospect; GT=granitoid-hosted type. Mineral =mineralization, NG=non-mineralized granitoid. ST=shear zone-hosted type (e.g. Ashanti type). 1P-a, -b and 1S-a, -b=primary and secondary H_2O -CO₂-rich ±NaCl fluid inclusions with VCO₂ <50% and >50% at room temperature, respectively. 2P, 2S=primary and secondary monophase gaseous CO₂-N₂-±CH₄ fluid inclusions, respectively. 3P=primary aqueous monophase liquid H₂O±NaCl fluid inclusions. Post-Mod.=post-entrapment modifications of fluid inclusions showing evidence of leakage and/or necking-down under microscope at room temperature, whereas in the case of the Sansu mine at Ashanti, it refers to post-entrapment modifications of fluid inclusions by grain boundary migration/recrystallization in the ductile and brittle transition.

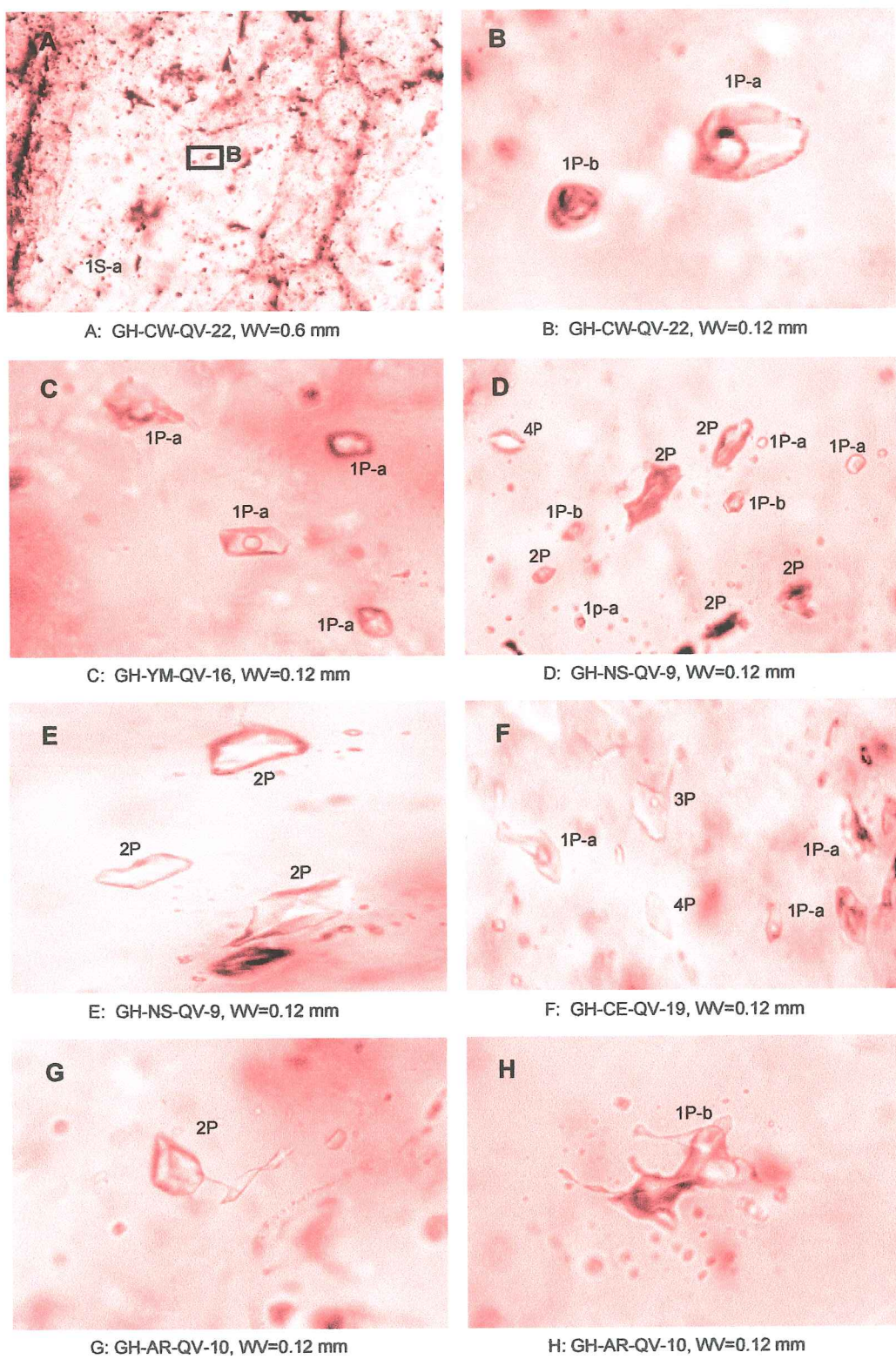


Figure 2. Photomicrographs of the major fluid inclusion types in vein quartz from Basin-type granitoid-hosted gold deposits and prospects in the Kumasi basin, Ghana. WV=width of view. 1P-a, 1P-b =primary 2- or 3-phase H_2O - CO_2 -rich±NaCl fluid inclusions with $V_{CO_2} < 50\%$ and $> 50\%$, respectively; 1S-a=secondary 2-phase H_2O - CO_2 -rich±NaCl fluid inclusions with $V_{CO_2} < 50\%$. 2P=primary monophase gaseous CO_2 - N_2 ± CH_4 fluid inclusions. 3P=primary 2-phase aqueous H_2O ±NaCl fluid inclusions. 4P=primary monophase aqueous liquid H_2O ±NaCl fluid inclusions. Note a 2P fluid inclusion in G showing micro-fractures that may represent paths of H_2O leakage, and textures of a 1P-b fluid inclusion in H possibly resulting from necking-down of fluid inclusions. Samples: GH=Ghana; QV=quartz vein; AR=Ayankyerim mine at Obuasi; NS=Nhyiaso mine at Obuasi; YM=Yamensakrom prospect at Obuasi. CE=Chirawewa East at Ayanfuri; CW=Chirawewa West at Ayanfuri.

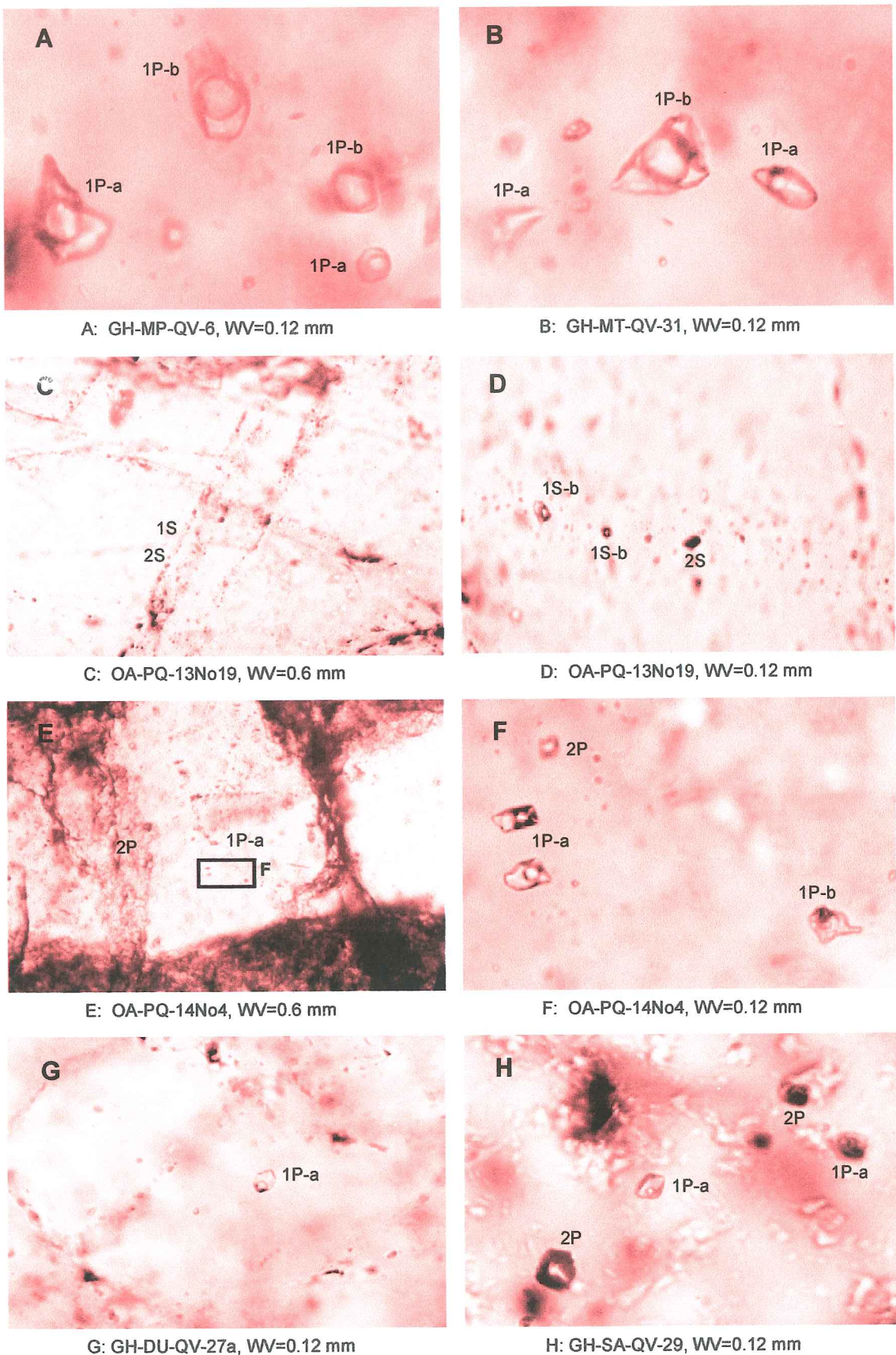


Figure 3. Photomicrographs of the major fluid inclusion types in vein quartz from Belt-type granitoid-hosted gold deposits and prospects in the Birimian of Ghana. 1S-b=secondary 2-phase H_2O-CO_2 -rich $\pm NaCl$ fluid inclusions with $V_{CO_2} > 50\%$. 2S=secondary monophase gaseous $CO_2-N_2\pm CH_4$ fluid inclusions. MP=Mporhor prospect in the Ashanti belt. MT=Mpesetia prospect in the Asankrangwa belt; OA-PQ-13No19, OA-PQ-14No4=borehole samples from the Abore North prospect in the Asankrangwa belt. DU=Dokrupe mine in the Bole-Navrongo belt; SA=Sakpa mine in the Bole-Navrongo belt. Abbreviations as in Fig. 2.

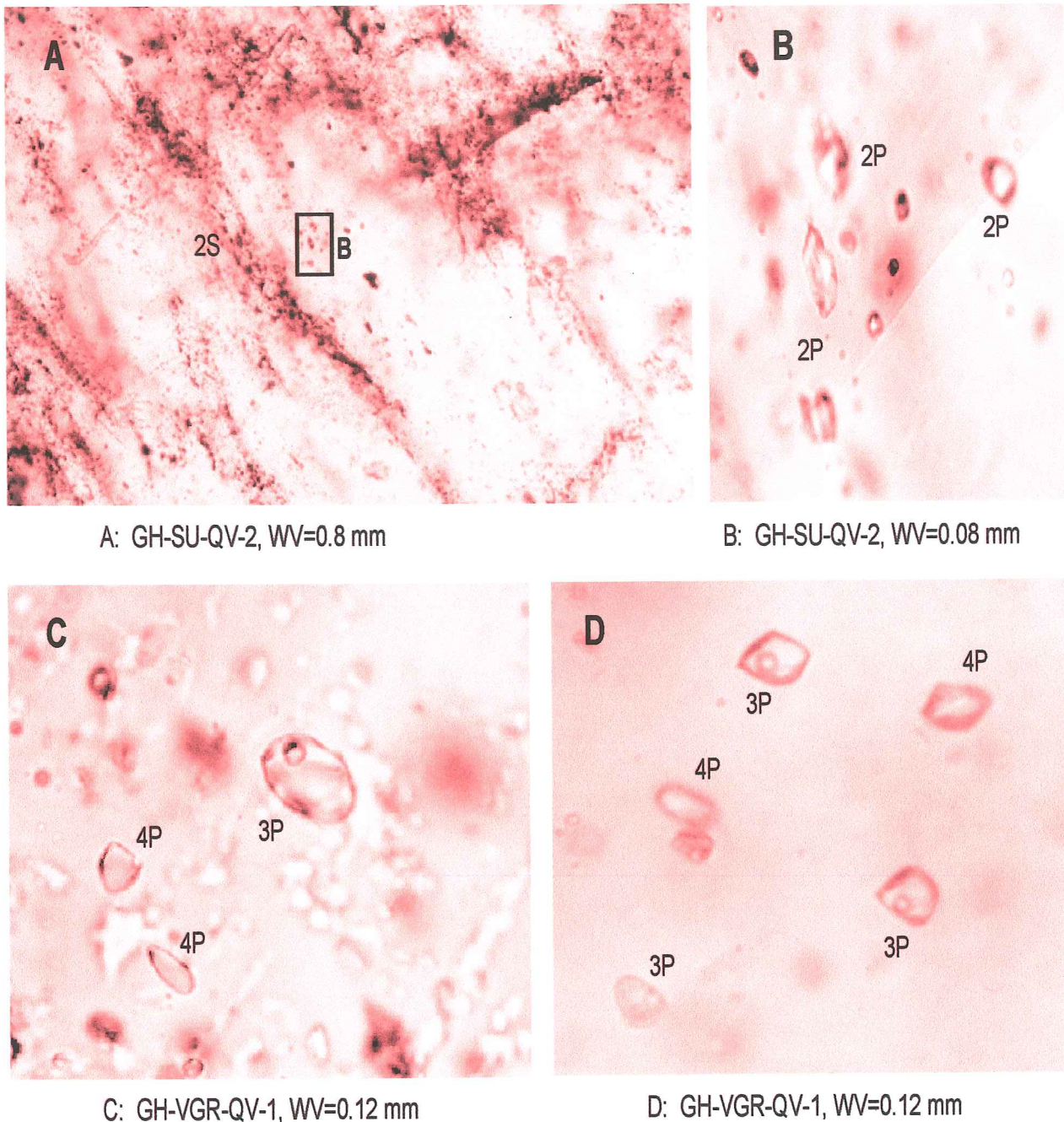


Figure 4. Photomicrographs of the major fluid inclusion types in vein quartz from the Sansu (SU) mine at Ashanti and in barren vein quartz from the non-mineralized granodiorite at Princess Town in the Birimian of Ghana. VGR=Belt-type granitoid in meta-volcanic rocks at Princess Town. Abbreviations as in Figs. 2, 3.

(1) Type 1: primary (1P) and secondary (1S) 2- or 3-phase $\text{H}_2\text{O}-\text{CO}_2\pm\text{NaCl}$ fluid inclusions. CO_2 phase volume proportions (V_{CO_2}), estimated at 25 °C, commonly show low V_{CO_2} (10 to 40%) and high V_{CO_2} (60 to 90%) groups. Hence, subtypes, defined by the V_{CO_2} , comprise 1P-a ($V_{\text{CO}_2} < 50\%$), 1P-b ($V_{\text{CO}_2} > 50\%$), 1S-a ($V_{\text{CO}_2} < 50\%$), and 1S-b ($V_{\text{CO}_2} > 50\%$) fluid inclusions (Fig. 2A-D, F; Fig. 3);

(2) Type 2: primary (2P) and secondary (2S) monophase gaseous $\text{CO}_2-\text{N}_2\pm\text{CH}_4$ fluid inclusions (Fig. 2D, E; Fig. 3D, F, H; Fig. 4A-B). These inclusions are generally dark and show no visible aqueous phase at 25 °C;

(3) Type 3: primary (3P) and secondary (3S) 2-phase aqueous $\text{H}_2\text{O}\pm\text{NaCl}$ fluid inclusions with vapor bubble volume ratios of commonly less than 10% (Fig. 2F; Fig. 4C-D). No CO_2 phase can be detected microthermometrically, although a very small amount of CO_2 may be present in certain of the fluid inclusions (Rosso and Bodnar, 1995);

(4) Type 4: primary (4P) monophase aqueous liquid $\text{H}_2\text{O}\pm\text{NaCl}$ fluid inclusions with no vapor bubbles observed at 25 °C. These inclusions are rarely found in samples from the gold deposits studied.

Types 1 and 2 constitute the majority of fluid inclusions in vein quartz within mineralized granitoids, while types 3 and 4 were mainly observed to occur as individual groups in barren vein quartz within the non-mineralized Princess Town granodiorite. By contrast, fluid inclusions in vein quartz from the Sansu mine are dominated by type 2.

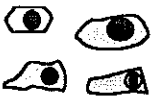
Primary fluid inclusions in all the studied samples commonly occur as randomly scattered groups comprising both type 1 and 2 inclusions (Fig. 2A-F, Figs. 3-4), although, in a few cases, type 1 or type 2 inclusions are also present in isolation (Fig. 3G). The fluid inclusions are both regular and irregular in shape, and some show negative crystal forms (Figs. 2-4). The sizes of primary fluid inclusions range from about 3 to 62 μm (commonly 8 to 25 μm ; Tables 1, 2). Secondary fluid inclusions of types 1 and 2 occur as small aggregates (Fig. 3D). They are commonly less than 15 μm in size, but some of them are as large as 68 μm in size (Tables 1, 2). Cross-cutting relationships among primary fluid inclusion types were not observed in the 16 samples studied, and the chronological sequence of primary fluid inclusion types cannot be recognized. As shown in Figs. 2-3, fluid inclusions of types 1P and 2P co-exist in individual arrays, implying that the different compositional types of primary fluid inclusions were probably coeval. Similarly, different types of secondary fluid inclusions are also observed to co-exist in trails (Fig. 2C, D), suggesting that they were trapped simultaneously.

Microthermometric data

A summary of microthermometric data for major fluid inclusion types from the granitoid-hosted gold deposits is presented in Table 2, while the detailed microthermometric data for fluid inclusions measured in the present study are presented in Tables 3 to 5 and plotted in Figures 5 to 11.

Granitoid-hosted gold deposits: Fluid inclusions in individual samples mainly comprise types 1 and 2, with only minor types 3 and 4 present. Type 1P fluid inclusions are present in all the studied samples and show various CO_2 volume proportions (V_{CO_2}), estimated at 25 °C, with X_{CO_2} values ranging from 0.005 to 0.21 for the 1P-a, and from 0.09 to 0.87 for the 1P-b. Samples from the Yamensakrom and Sakpa gold deposits, however, principally display 1P-a fluid inclusions with X_{CO_2} values of 0.02 to 0.20 and 0.01 to 0.19, respectively. Melting temperatures of the CO_2 phase ($T_m\text{CO}_2$) are between -62.7 and -57.3 °C for the 1P-a, and -61.6 and -57.4 °C for the 1P-b (Table 2, Fig. 5a, e). These temperatures are about 0.7 to 6 °C lower than the pure CO_2 melting point (-56.6 °C), indicating the presence of additional volatile species. Melting temperatures of CO_2 clathrate (T_{mclath}) are between 2.4 and 14.2 °C for the 1P-a, and between 3.1 and 11.2 °C for the 1P-b (Table 2, Fig. 5b, f). From these results, the estimated salinities fall in a range from 0 to 12 wt.% NaCl equivalent, clustering at 0 to 6 wt.% NaCl equivalent for the 1P fluid inclusions. The presence of additional gases in the carbonic phase implies that the salinities estimated from T_{mclath} values represent minima (Diamond, 1994). The carbonic portion of most of the 1P-a and 1P-b fluid inclusions homogenized into the liquid phase, and their $T_h\text{CO}_2(L)$ values span a range from -11.8 to 28.9 °C for the 1P-a and from -41.6 to 30.6 °C for the 1P-b (Fig. 5c, g, one value of -41.6 °C in Fig. 5g not shown), respectively. In some cases, however, the carbonic part of 1P inclusions

Table 2. Summary of petrographic and microthermometric data for fluid inclusions from granitoid-hosted gold deposits in Ghana.

Type	System	Occurrence	Size (μm)	Microthermometric data
1P-a	H ₂ O-rich-CO ₂ -NaCl		3 to 62	T _m CO ₂ : -62.7 to -57.3 °C; T _{mclath} : 2.4 to 14.2 °C; T _h CO ₂ (L): -11.8 to 28.9 °C; T _h CO ₂ (V): -15.6 to 26.9 °C; T _h (L): 161 to 379 °C (mostly decrepitate); salinity: 0 to 12 wt.% (commonly 0 to 6 wt.%); ρ _c : 0.05 to 0.97 g/cm ³ ; X _{CO₂} : 0.005 to 0.21.
1P-b	H ₂ O-CO ₂ -rich-NaCl		5 to 50	T _m CO ₂ : -61.6 to -57.4 °C; T _{mclath} : 3.1 to 11.2 °C; T _h CO ₂ (L): -41.6 to 30.6 °C; T _h CO ₂ (V): 5.5 to 27.5 °C; T _h (L): 161 to 387 °C (mostly decrepitate); salinity: 0 to 12 wt.% (commonly 0 to 6 wt.%); ρ _c : 0.11 to 1.12 g/cm ³ ; X _{CO₂} : 0.09 to 0.87.
1S-a	H ₂ O-rich-CO ₂ -NaCl		5 to 54	T _m CO ₂ : -61.0 to -57.8 °C; T _{mclath} : 8.1 to 11.2 °C; T _h CO ₂ (L): -10.2 to 26.7 °C; T _h (L): 121 to 310 °C (mostly decrepitate); salinity: 0 to 3.8 wt.%; ρ _c : 0.68 to 0.98 g/cm ³ ; X _{CO₂} : 0.01 to 0.21.
2P	CO ₂ -N ₂ -CH ₄		3 to 56	T _m : -97.1 to -57.0 °C (commonly -60.0 to -58.0 °C); T _h CO ₂ (L): -14.8 to 29.8 °C; T _h CO ₂ (V): -58.3 to 25.5 °C; ρ _b : 0.30 to 0.92 g/cm ³ ; CO ₂ *: 63 to 97 mol%.
2S	CO ₂ -N ₂ -CH ₄		4 to 68	T _m : -59.6 to -57.8 °C; T _h CO ₂ (L): -36.8 to 24.7 °C.
3P	H ₂ O-NaCl		4 to 30	T _e : -53.2 to -16.7 °C; T _{m-ice} : -4.8 to -0.5 °C; T _h (L): 181 to 316 °C (some decrepitate); salinity: 0.9 to 7.6 wt.%; ρ _b : 0.77 to 1.03 g/cm ³ ; X _{H₂O} : 0.98 to 1.00.

Note: T_mCO₂=melting temperature of CO₂ phase; T_{mclath}=dissolution temperature of CO₂-clathrate; T_hCO₂(L), (V)=homogenization temperature of CO₂ phase into the carbonic liquid and vapor phases, respectively; T_h(L), (V)=total homogenization temperature into the aqueous fluid and carbonic vapor phases, respectively; T_m=melting temperature of solid CO₂ phase for gaseous fluid inclusions; T_e=first melting temperature of eutectic phases; T_{m-ice}=final melting temperature of ice; ρ_c=density of carbonic phase; ρ_b=density of bulk fluid inclusions; X_{CO₂}, X_{H₂O}=mole fractions of CO₂ and H₂O, respectively; CO₂*=CO₂ in mol% estimated from Raman analyses of gaseous fluid inclusions.

homogenized into the vapor phase, with T_hCO₂(V) values in the range from -15.6 to 26.9 °C for the 1P-a (n=36) and from 5.5 to 27.5 °C for the 1P-b (n=22). Estimated CO₂ densities cover a wide range from 0.05 to 0.97 g/cm³ for the 1P-a and from 0.11 to 1.12 g/cm³ for the 1P-b, respectively. More than 90% of the CO₂ densities cluster at 0.77 to 0.96 g/cm³ for the

Table 3. Summary of microthermometric and Raman spectrometric data for fluid inclusions from mineralized Basin granitoids at Obuasi and Ayanfuri in the Kumasi Basin

Table 3. (continued)

Deposit/prospect	Fl type	Issue	N	VCO ₂ /N/b	T _i	TmCO ₂ /	T _e	Tm-ice	T _m cath	ThCO ₂ (L)	ThCO ₂ (V)	Th(L)	Th(V)	Td	Salinity	pCO ₂	ρ _b	XH ₂ O	XNaCl	XC _{CO₂}	C _{O₂} ⁻	N ₂ [*]	CH ₄ [*]	mol%	mol%	mol%	mol%
(sample)					(°C)	(°C)	(°C)	(°C)	(°C)	(°C)	(°C)	(°C)	(°C)	(°C)	(°C)	wt% NaCl	g/cm ³										
Ayankyerim, Obiasi (GH-AR-QV-10 + GH-AR-QV-14)	1S-b	Min	60	-58.3	8.2	0.6	2.5			167	2.6	0.97	0.94	0.3824	0.0033	0.3613											
	Max	80	-58.0	8.7	3	3				279	3.6	0.92	0.96	0.6315	0.0073	0.6044											
	N	14	-64.4	-59.6						14	3	3	3	3	3	3											
	Min	59.1	-58.4							23.9																	
	Max	31	33	-39.4	-4.8					36																	
	3P	Min	13	-16.7	-0.7					180	1.2																
	Max	N	N	21					10	8	21	10	10	10	10	10											
Chirawewa East, Ayanturi (GH-CE-QV-19)	1P-a	Min	5	-61.2	7.8	-3.5	5.2	171		156	0.0	0.12	0.66	0.7583	0.0000	0.0118	0.92	5	0								
	Max	40	-59.2	10.2	22.6	8.3	339		323	4.3	0.95	1.00	0.9863	0.0121	0.1897	0.96	8	0.5									
	N	141	105	114	2	14			83	114	116	102	102	102	102												
	Min	60	-59.8	7.4	-3.3				351	156	0.4	0.73	0.79	0.2317	0.0022	0.3230		3	3								
	Max	95	-58	9.8	23.5				283	5.1	0.95	0.6683	0.0038	0.7650													
	2P	Min	34	33	23	26			13	23	26	19	19	19	19												
	Max	-63.8	-59.6						24.3	20.6	24.3	21.7	24.3	21.7	24.3												
	N	-60.4	-57.3						35	2	35	2	35	2	35												
	3P	Min	1	3	38	-4.5				166	1.4																
	Max	30		-0.8					274	7.2	274	7.2	274	7.2	274												
	N	20		-2.0					2	20	2	20	20	20	20												
	4P	Min		-3.0						2	2.1	2.1	2.1	2.1	2.1	2.1											
	Max			-1.2						5.0	1.03	0.9835	0.0056	0.9835	0.0159	0.9518											
	N			2						2	2	2	2	2	2	2											
Chirawewa West, Ayanturi (GH-CW-QV-22)	1P-a	Min	5	-60.7	7.7	-3.7	8.5	209		168	0.0	0.13	0.65	0.7903	0.0000	0.0181											
	Max	40	-57.9	10.1	26.9	35.9			277	4.5	0.95	1.00	0.9756	0.0139	0.2045												
	N	109	91	95	6	14			26	96	91	89	89	89	89												
	Min	60	-61.5	7.7	-7.6				285	159	0.6	0.19	0.27	0.1388	0.0006	0.1702											
	Max	95	-58	9.7	26.8				364	26.2	4.5	0.97	0.98	0.8219	0.0089	0.8621											
	2P	Min	79	72	67	67			9	19	67	72	57	57	57												
	Max	-51.6	-59.7						27.3	24.1	27.3	24.1	27.3	24.1	27.3												
	3P	Min	5	68	79	-0.5			79	2	79	2	79	2	79		0.9	1.0	0.9973	0.0027							
	Max	N	1	1	1						1	1	1	1	1	1											

Note: Fl=fluid inclusion, Max=maximum, Min=minimum, N=natural, 1P-a, 1P-b=primary 2- or 3-phase H₂O-CO₂-NaCl fluid inclusions with VCO₂<50% and >50%, respectively, 1S-a and 1S-b=secondary 2-phase H₂O-CO₂-NaCl fluid inclusions with a visible aqueous phase at room temperature, 2P, 2S-primary and secondary monophase gaseous CO₂-N₂±CH₄ fluid inclusions without a visible aqueous phase, 3P=primary aqueous 2-phase liquid H₂O±NaCl fluid inclusions, 4P=aqueous monophase liquid H₂O±NaCl fluid inclusions, Td=decrepitation temperature, Te=eutectic temperature of solid CO₂ phase, Tm=final melting temperature of solid CO₂ phase for 2P fluid inclusions, Th=homogenization temperature of CO₂ phase into the carbonic liquid and vapour phases, respectively, Th(L)=total homogenization temperature of the aqueous fluid and carbonic vapor phases, respectively, Tm-ice=dissolution temperature of CO₂ clathrate, TmCO₂=melting temperature of CO₂ phase, Th(V)=decrepitation temperature of CO₂ phase, Th(V')=melting temperature of CO₂ phase, T_i=initial melting temperature of ice, T_mcath=dissolution temperature of CO₂ clathrate, ρ_b=bulk density of fluid inclusions, pCO₂=carbonic density of fluid inclusions, V_b=volume percent of vapor bubbles estimated at 25 °C, VCO₂=carbonic volume percent estimated at room temperature, XH₂O, XNaCl, and XC_{CO₂}=mole fractions of H₂O, NaCl, and CO₂, N₂^{*}, and CH₄^{*}=mole% CO₂, N₂, and CH₄ estimated from microthermometric data, CO₂^{*}, N₂^{*}, and CH₄^{*} estimated from Raman analysis.

Table 4. Summary of microthermometric and Raman spectrometric data for fluid inclusions from mineralized Belt granitoids in the volcanic belts

Deposit/prospect	Fl type:	Issue	N	VCO ₂	T _i	T _{mCO₂/T_m}	T _{hs/} T _m	T _e	T _{m-ice}	T _{m-clath}	T _{CO₂(L)}	T _{CO₂(V)}	T _{h(L)}	T _{h(V)}	T _d	Salinity	ρ_{CO_2}	ρ_b	XH ₂ O	XNaCl	XCO ₂	CO ₂ ⁻	N ₂ ⁻	CH ₄ ⁻	mol% mol%	mol% mol%	
Mporhor (AT) (MP-QV-6)	1P-a	Min	5	-59.7	6.8	-11.8	10.2	28.9	37.9	30.9	6.1	0.0	0.63	0.87	0.7840	0.0000	0.0172	94	0.3	0	0	0	0	0	0	0	
	Max	40	-58.0	61	59	-15.3	27.5	9	286	156	61	59	0.0	0.59	1.02	0.9757	0.0189	0.2129	98	1	0	0	0	0	0	0	0
	N	64	44	-61.0	6.8	-10.9	10.9	30.6	374	319	6.1	0.28	0.51	0.2104	0.0000	0.2122	95	0.4	0	0	0	0	0	0	0		
	1P-b	Min	60	-58.1	50	51	1	-14.8	23.3	9	45	52	52	52	52	52	52	52	52	4	4	4	4	4	4	4	4
	Max	90	54	-58.9	-58.6	45	8.3	-10.2	26.7	2	121	0.2	0.68	0.99	0.9066	0.0012	0.0146	97	4	0.5	0.5	0.5	0.5	0.5	0.5	0.5	
	2P	Min	20	-58.1	-58.9	2	9.9	26.7	188	3.4	11	12	11	0.98	1.00	0.9784	0.0010	0.0923	3	3	3	3	3	3	3	3	
	Max	12	-59.0	-59.5	16	-1.4	-24.7	24.7	16	7	7	7	7	7	7	7	7	7	7	7	7	7	7	7	7		
	1S-a	Min	5	-59.0	-59.5	2	-1.4	-24.7	24.7	16	7	7	7	7	7	7	7	7	7	7	7	7	7	7	7		
	Max	20	-59.0	-59.5	16	-1.4	-24.7	24.7	16	7	7	7	7	7	7	7	7	7	7	7	7	7	7	7			
	2S	Min	12	-59.0	-59.5	2	-1.4	-24.7	24.7	16	7	7	7	7	7	7	7	7	7	7	7	7	7	7	7		
	Max	N	N	N	N	N	N	N	N	N	N	N	N	N	N	N	N	N	N	N	N	N	N	N	N		
Mposetta (AS) (GH-MT-QV-31)	1P-a	Min	10	-64.7	-61.3	9.7	1.2	5.7	214	298	169	0.0	0.12	0.90	0.7978	0.0000	0.0053	81	1	4	4	4	4	4	4	4	
	Max	40	-59.9	-50.7	11.1	19.8	11.5	375	389	317	66	0.32	0.38	0.5947	0.0017	0.2022	94	13	6	6	6	6	6	6	6		
	N	69	33	59	66	58	3	5	52	52	61	61	61	61	61	61	61	61	61	7	7	7	7	7	7	7	7
	1P-b	Min	60	-66.0	-61.6	9.9	-2	339	388	172	0.00	0.75	0.82	0.2226	0.0000	0.3233	92	1	5	5	5	5	5	5	5		
	Max	90	-60.5	-59.3	11.2	22	22	387	317	0.21	0.94	0.96	0.5737	0.0004	0.7774	94	3	6	6	6	6	6	6	6			
	N	22	53	64	64	64	6	64	64	64	64	64	64	64	64	64	64	64	64	4	4	4	4	4	4	4	4
	2P	Min	-65.1	-61.4	-61.4	-61.4	-61.4	-1.1	18.5	227	172	0.00	0.86	0.86	0.86	0.0000	0.0191	0.98	3	6	6	6	6	6	6	6	
	Max	N	-61.8	-59.2	-59.2	-59.2	-59.2	-6	249	301	0.00	0.91	0.91	0.91	0.0000	0.1370	0.91	5	7	7	7	7	7	7	7		
	1S-a	Min	5	-61.0	-61.0	-61.0	-61.0	-61.0	10.4	3.6	227	0.00	0.86	0.86	0.86	0.0000	0.0191	0.98	3	6	6	6	6	6	6	6	
	Max	30	6	-60.2	-60.2	-60.2	-60.2	-60.2	11.2	10.8	249	2	0.00	0.88	0.88	0.88	0.0000	0.3564	0.91	5	7	7	7	7	7	7	
	N	8	7	7	7	7	7	7	6	5	2	0.00	0.93	0.93	0.93	0.0000	0.4589	0.91	5	7	7	7	7	7	7		
	1S-b	Min	60	-61.4	-61.4	-61.4	-61.4	-61.4	10.7	-1.0	189	0.00	0.93	0.93	0.93	0.0000	0.4589	0.91	5	7	7	7	7	7	7	7	
	Max	70	70	-60.2	-60.2	-60.2	-60.2	-60.2	10.9	6.9	232	0.00	0.93	0.93	0.93	0.0000	0.4589	0.91	5	7	7	7	7	7	7	7	
	N	3	2	2	2	2	2	2	2	2	3	2	2	2	2	2	2	2	2	2	2	2	2	2	2		
	2P	Min	5	-62.7	-49.7	2.4	-5.5	18.2	231	221	0.0	0.18	0.75	0.5863	0.0000	0.0310	35	0	1	1	1	1	1	1	1		
	Max	40	-57.3	-44.2	14.2	16.0	35	42	1	6	181	181	181	181	181	181	181	181	181	13	13	13	13	13	13	13	13
	N	57	36	26	3	-55.3	-55.3	-55.3	-55.3	-55.3	1	1	1	1	1	1	1	1	1	1	1	1	1	1	1	1	
	1P-b	Min	2	-60.7	-53.2	1	1	-53.2	-3.4	-3.4	-3.4	-0.5	-0.5	-0.5	-0.5	-0.5	-0.5	-0.5	-0.5	5.6	5.6	5.6	5.6	5.6	5.6	5.6	5.6
	3P	Min	1	1	1	1	1	1	1	1	1	1	1	1	1	1	1	1	1	1	1	1	1	1	1	1	
	Max	N	N	N	N	N	N	N	N	N	N	N	N	N	N	N	N	N	N	N	N	N	N	N	N		
	3S	Min	2	-60.7	-53.2	1	1	-53.2	-3.4	-3.4	-3.4	-0.5	-0.5	-0.5	-0.5	-0.5	-0.5	-0.5	-0.5	5.7	5.7	5.7	5.7	5.7	5.7	5.7	5.7
	Max	N	N	N	N	N	N	N	N	N	N	N	N	N	N	N	N	N	N	N	N	N	N	N	N		
	Above North (AS) (OA-PQ-13N19+ OA-PQ-8N6)	1P-a	Min	5	-62.7	-49.7	2.4	-5.5	18.2	376	321	12.7	0.96	0.95	0.95	0.9571	0.0019	0.1387	95	64	9	9	9	9	9	9	9
	Max	40	-57.3	-44.2	14.2	16.0	35	42	1	6	24	36	44	24	24	24	24	24	24	24	24	24	24	24	24	24	
	N	57	36	26	3	-55.3	-55.3	-55.3	-55.3	-55.3	1	1	1	1	1	1	1	1	1	1	1	1	1	1	1		

Table 4. (Continued)

Deposit/prospect	Fl type	Issue	N	VCO ₂	T _i	T _{mCO₂/Tm}	T _{hs}	T _e	T _{m-ice}	T _{mclath}	T _{CO₂(V)}	T _{h(L)}	T _{h(V)}	T _d	Salinity	pCO ₂	XH ₂ O	XNaCl	XCO ₂	p _b	XH ₂ O	mol% NaCl	mol% CO ₂	N ₂ '	CH ₄ '	mol% mol%
Dokrupe (BN)	1P-a	Min	10	-61.2	7.1	2.7	166	206	0.2	0.82	0.95	0.7887	0.0026	0.0385	85	9	2									
GH-DU-QV-27+		Max	40	-58.4	9.9	15.4	374	313	5.6	0.51	1.00	0.9546	0.0151	0.2006	88	10	5									
GH-DU-QV-2		N	130	84	100	49	40	62	100	49	49	49	49	49	49	2	2	2								
1P-b	Min	60	-61	8.5	0.8			217	0.8	0.87	0.90	0.3956	0.0017	0.3542												
	Max	90	-60.2	9.6	9			316	3.0	0.82	0.95	0.6442	0.0044	0.5391												
	N	4	4	4	4			4	4	4	4	4	4	4	4	4	4	4	4	4	4	4	4	4		
2P	Min	-60.7	-60.7	-3.4																						
	Max	-59.3	-59.3	6.6																						
	N	8	8	8																						
Sakpa (BN)	1P-a	Min	5	-59.6	3.2	13.7	207	217	7.9	0.22	0.32	0.7872	0.0029	0.0098												
GH-SA-QV-28		Max	40	-58.1	5.7	27.3	267	297	11.7	0.83	1.04	0.5651	0.0380	0.1659												
		N	42	25	27	25	18	21	27	25	25	25	25	25	25	25	25	25	25	25	25	25	25	25		
1P-b	Min	60	-58.2	3.1	22			217	11.8	0.75	0.88	0.6550	0.0270	0.3179												
	Max	60	2	1	1			234	2	1	1	1	1	1	1	1	1	1	1	1	1	1	1	1		
	N	2	1	1	1																					

Note: Ths=partial homogenization temperature and sublimation of gaseous fluid inclusions, respectively. Abbreviations as in Table 3.

Table 5. Summary of microthermometric and Raman spectrometric data for fluid inclusions from the Sansu mine at Ashanti and from the non-mineralized granodiorite at Princess Town

Deposit/area (sample)	Fl type	Issue	N	T _i	T _m	T _e	T _m -ice	T _{h(L)}	Salinity (wt%)	p _b	XH ₂ O	XNaCl	XCO ₂ *	CO ₂ *	N ₂ *	CH ₄ *
					(°C)	(°C)	(°C)	(°C)	NaCl equiv.)	g/cm ³				mol%	mol%	mol%
Sansu (GH-SU-QV-2)	2P	Min	-66.5	-61.8				-32.6		0.83	0	0		90	3	0.4
		Max	-58.5	-57.7				13.6		0.96	0	0		96	10	1
		N	50	63				80		8	8	8		8	8	8
2S	2S	Min	-63.2	-59.5				-30.3								
		Max	-59.8	-58.7				-0.9								
		N	13	15				17								
Princess Town (VGR-QV-1)	3P	Min			-58.6	-6.3			0.0	0.99	0.9683	0.0000		0		
		Max			-21.4	1.2			9.6	1.06	1.0000	0.0317		0		
		N			25	91			91	91	91	91		91		
4P	4P	Min			-49.5	-6.3			0.0	0.99	0.9683	0.0000		0		
		Max			-31.9	1.4			9.6	1.06	1.0000	0.0317		0		
		N			6	43			43	43	43	43		43		

Note: Abbreviations as in Table 3.

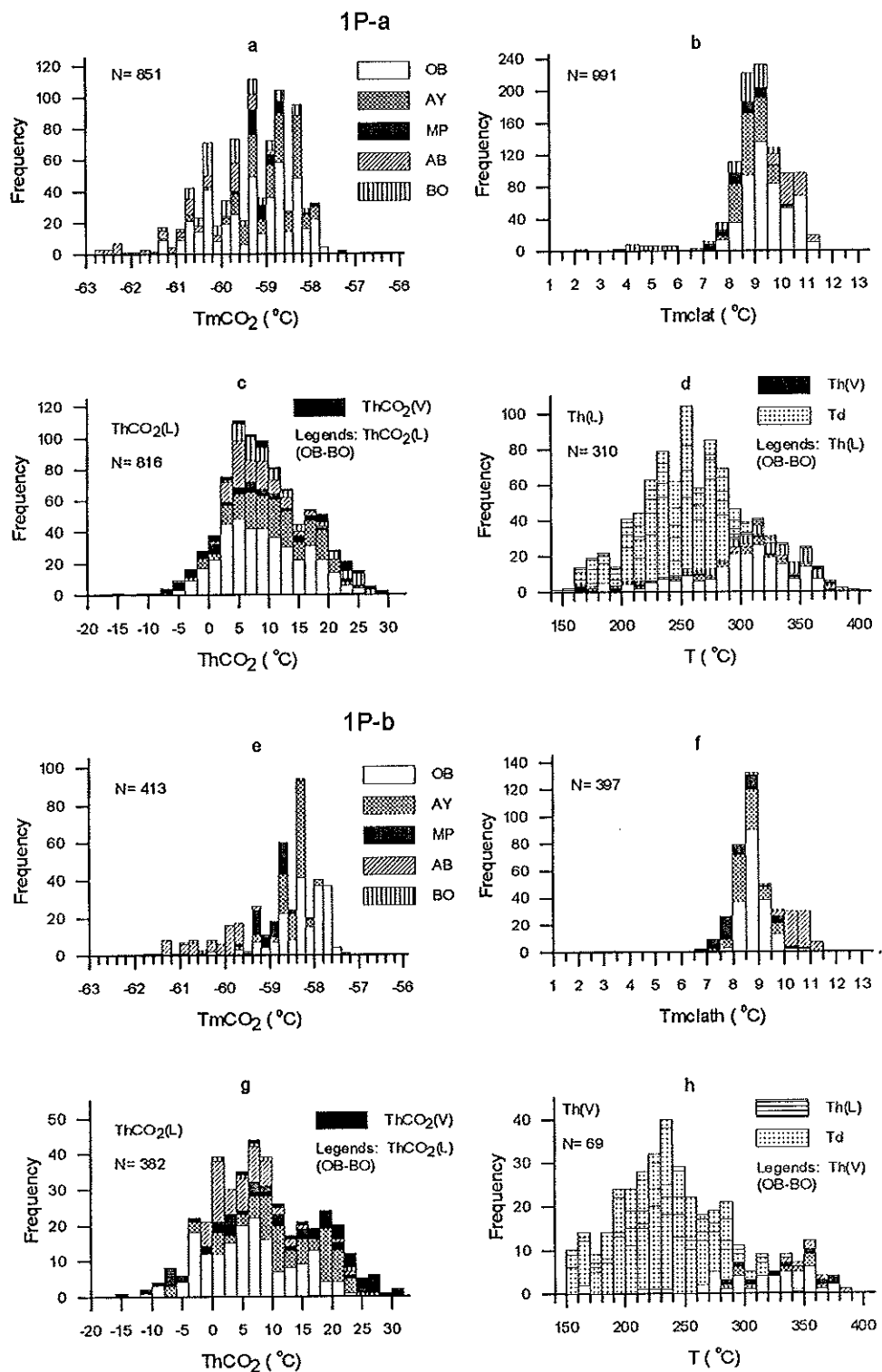


Figure 5. Frequency- T_{mCO_2} , - T_{mclath} , - $ThCO_2$, and -T histograms of IP-a and IP-b fluid inclusions in vein quartz from granitoid-hosted gold deposits and prospects in Ghana. T_{mCO_2} =melting temperature of CO_2 phase, T_{mclath} =dissolution temperature of CO_2 -clathrate, $ThCO_2(L)$, (V)=homogenization temperature of CO_2 phase into the liquid and vapor phases, respectively, T=temperature, $T_h(L)$ and $T_h(V)$ =total homogenization temperature into the aqueous fluid and the carbonic vapor phases, respectively, Td=decrepitation temperature. OB=Obuasi, Kumasi basin, AY=Ayanfuri, Kumasi basin, MP=Mporhor, Ashanti belt, AB=Abore, Asankrangwa belt, BO=Bole, Bole-Navrongo belt.

1P fluid inclusions. About 35% of 1P-a fluid inclusions homogenized into the aqueous fluid phase ($T_h(L)$) at 160 to 370 °C, clustering at 200 to 350 °C (Fig. 5d), and about 20% of 1P-b fluid inclusions homogenized into the carbonic vapor phase ($T_h(V)$) at 165 to 380 °C, with a common temperature range of 210 to 350 °C (Fig. 5h). The other 1P-a and 1P-b fluid inclusions decrepitated at 147 to 336 °C and 154 to 336 °C, respectively (Fig. 5d, h). The bulk density (ρ_b) of 1P-a inclusions falls in a range from 0.62 to 1.02 g/cm³ (n=826), and that of 1P-b inclusions from 0.23 to 1.11 g/cm³ (n=371) (Tables 2-4). X_{H_2O} and X_{NaCl} values range from 0.79 to 0.99, and 0 to 0.02 for the 1P-a, and from 0.13 to 0.91, and 0 to 0.02 for the 1P-b, respectively (Tables 3-4).

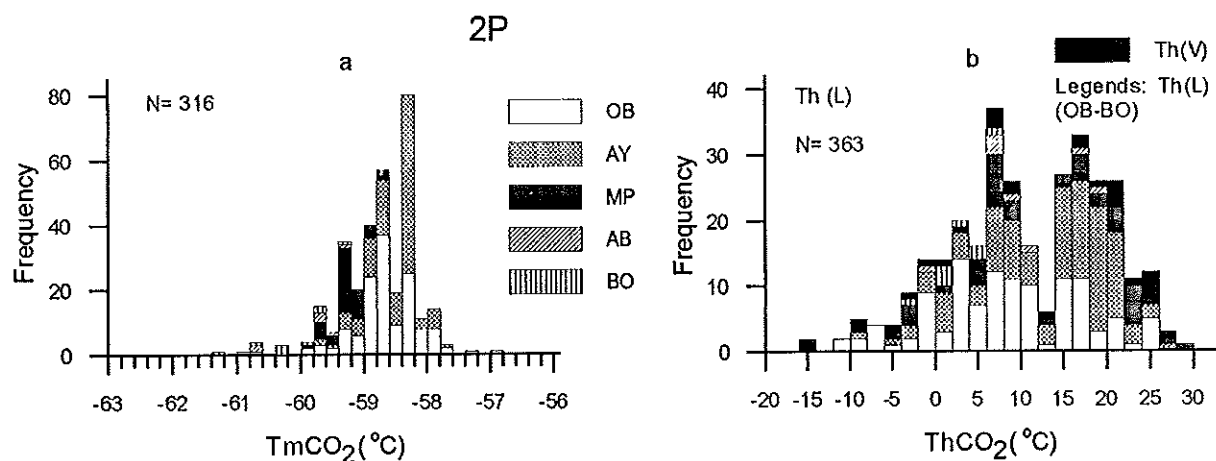


Figure 6. Frequency- T_mCO_2 and - $ThCO_2$ histograms of 2P fluid inclusions in vein quartz from granitoid-hosted gold deposits and prospects in Ghana. Abbreviations as in Fig. 5.

Type 2P fluid inclusions display a wide range of melting temperatures of solid CO₂ phase (T_mCO_2) from -61.3 to -57.0 °C, clustering at -60 to -58.0 °C (Fig. 6a). Most of the measured 2P fluid inclusions (n=314) correspond to the H₃ types, which show phase transition

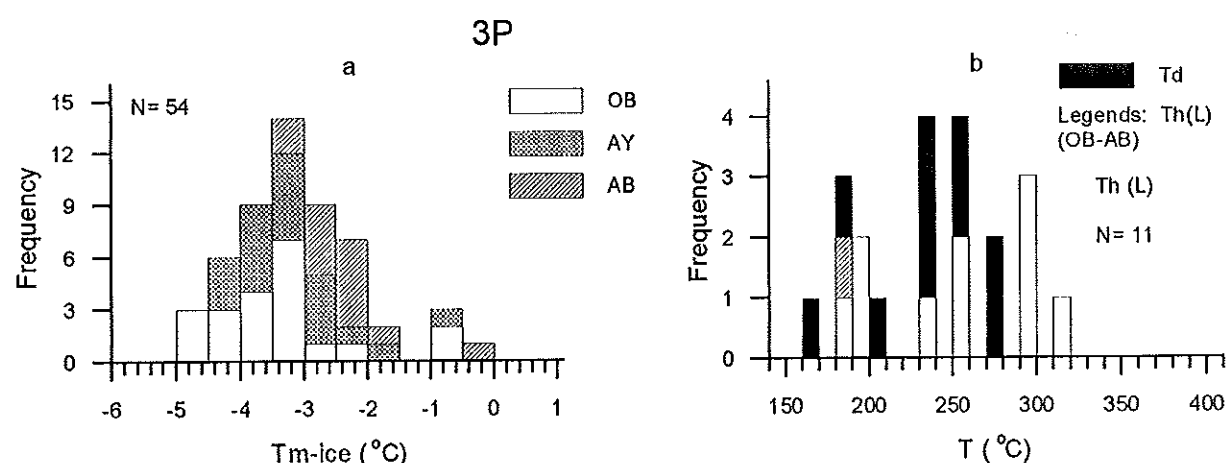


Figure 7. Frequency- T_{m-ice} and -T histograms of 3P fluid inclusions in vein quartz from granitoid-hosted gold deposits and prospects in Ghana. T_{m-ice} =melting temperature of ice. Abbreviations as in Fig. 5.

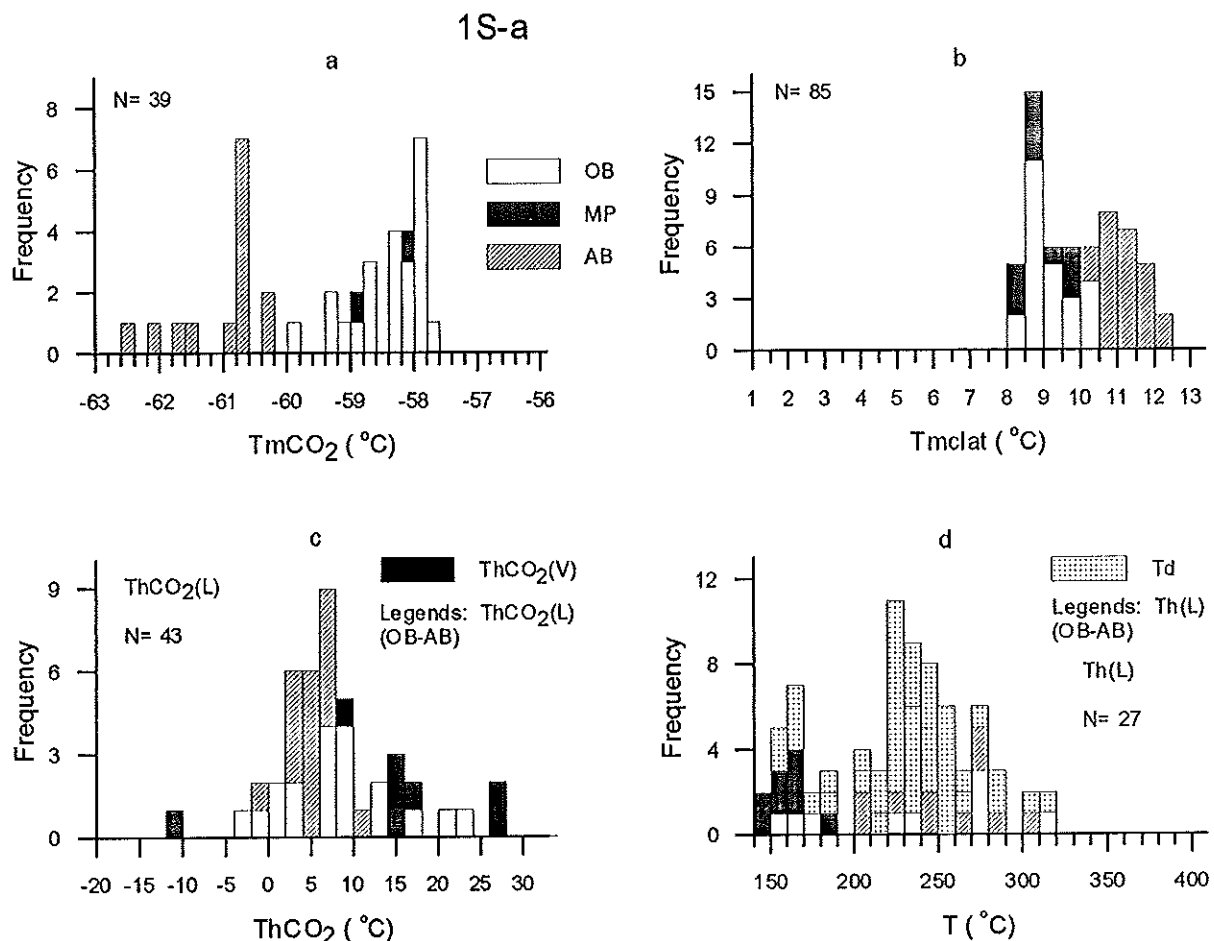


Figure 8. Frequency- $T_{m\text{CO}_2}$, - $T_{m\text{clath}}$, - ThCO_2 , and -T histograms of 1S-a fluid inclusions in vein quartz from granitoid-hosted gold deposits and prospects in Ghana. Abbreviations as in Fig. 5.

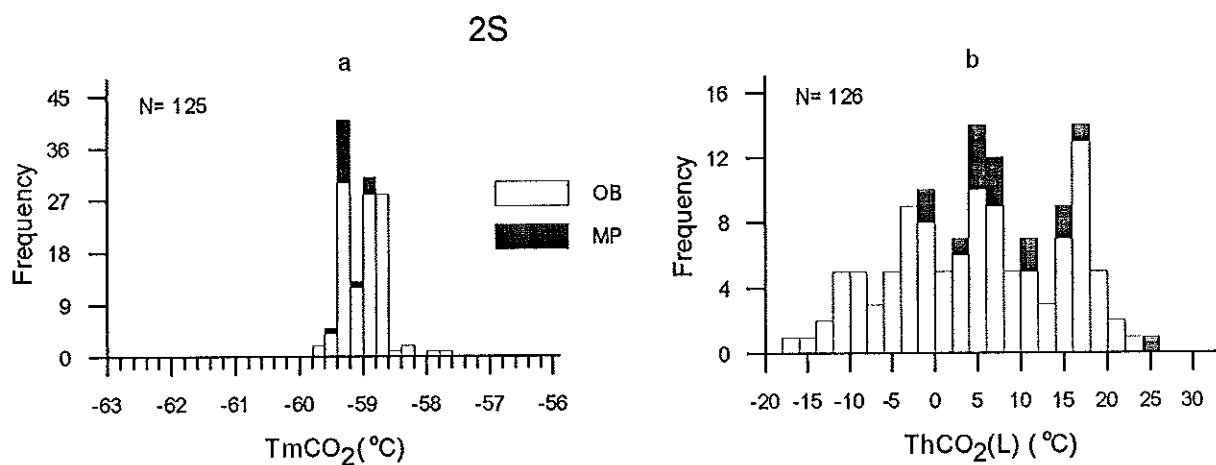


Figure 9. Frequency- $T_{m\text{CO}_2}$ and - ThCO_2 histograms of 2S fluid inclusions in vein quartz from granitoid-hosted gold deposits and prospects in Ghana. Abbreviations as in Fig. 5.

temperatures following the order from T_i (first melting temperature of solid phases), T_m (melting temperature of solid phases) to T_h (homogenization temperature of gaseous phase; van den Kerkhof, 1988). Only two fluid inclusions are the H_2 type (phase transition: T_m and T_h , van den Kerkhof, 1988), showing the T_m at -97.1 and -82.3 °C (not shown in Fig. 6a). T_i values of 2P fluid inclusions (H_3 type) are between -65.9 and -58.3 °C, indicating the presence of additional gases. Most of the 2P fluid inclusions homogenized into the carbonic liquid phase ($T_hCO_2(L)$) at temperature from -14.8 to 29.8 °C (Fig. 6b), and a few 2P inclusions (n=26) homogenized into the carbonic vapor phase ($T_hCO_2(V)$) at temperature from -58.3 and 25.5 °C (Fig. 6b, -58.3 °C not shown), indicating various bulk densities of the fluid inclusions. Limited 2P fluid inclusions with compositions determined by Raman show a wide range of bulk density (ρ_b) from 0.30 to 0.92 g/cm³ (Tables 2-4).

In one sample from the Nhyiaso open pit at Obuasi (GH-NS-GR-31), fluid inclusions in recrystallized parts of quartz grains are mostly the gaseous type, designated as 2P (RQ). These fluid inclusions are considered to represent post-entrapment modifications of primary ones with H_2O leakage during recrystallization of quartz grains. The T_mCO_2 (-59.4 to -57.9 °C) and T_hCO_2 (-9.6 to 15.6 °C) values of the 2P (RQ) fluid inclusions are comparable with those of the 2P fluid inclusions (Tables 2-3). The similarity of microthermometric data between the 2P (RQ) and 2P fluid inclusions implies that the H_2O leakage of 2P (RQ) fluid inclusions may not significantly affect the phase transition temperature.

Type 3P fluid inclusions were measured from Ayankyerim at Obuasi, Chirawewa East at Ayanfuri, and Abore North at Abore (Tables 3-4). First melting temperatures of eutectic phases (T_e) of the 3P inclusions were hard to detect due to the small size of eutectic crystals. The measured T_e values range from -53.2 to -16.7 °C (n=15), suggesting various amounts of Na^+ , K^+ , Ca^{2+} and Mg^{2+} cations in the inclusion fluid. It must be noted, however, that these cations are only qualitative to aqueous compositions of inclusion fluids due to uncertainty of measurements for the T_e . Final melting temperatures of ice (T_{m-ice}) fall in a narrow range from -4.8 to -0.5 °C (Fig. 7a), corresponding to salinities from 0.9 to 7.6 wt.% NaCl equivalent. Some 3P fluid inclusions homogenized into the aqueous fluid phase at temperatures of 181 to 316 °C, and some decrepitated at temperatures of 166 to 276 °C (Fig. 7b). These temperatures are comparable with those from the 1P fluid inclusions (Fig. 5d, h).

As shown in Tables 2-4 and Figs. 8-9, secondary 1S-a and 2S fluid inclusions are microthermometrically similar to their primary counterparts, although there is a tendency for lower homogenization temperatures in the secondary inclusions (Figs. 5d, h and 6b). These microthermometric results suggest that the ore-forming fluids remained relatively homogeneous and were internally buffered during what appears to have been a protracted mineralization sequence.

Sansu mine at Ashanti: Fluid inclusions are dominantly monophase gaseous type 2, with few, if any, aqueous $H_2O-CO_2\pm NaCl$ and $H_2O\pm NaCl$ inclusions observed in the studied sample (GH-QV-SU-2). Melting temperatures of the solid CO_2 phase (T_mCO_2) range from -61.8 to -57.7 °C for the 2P, and from -59.5 to -58.7 °C for the 2S (Fig. 10a). The T_mCO_2 values of 2P fluid inclusions show two groups: one at -61.3 to -60.3 °C and the other at -59.7 to -59.4 °C (Fig. 10a), which may reflect variations of other gaseous species (N_2 , CH_4) in the inclusions. Homogenization temperatures into the CO_2 liquid phase ($T_hCO_2(L)$) fall in a wide range from -32.6 to +13.6 °C for the 2P and from -30.3 to -0.9 °C for the 2S (Fig. 10b), indicating extreme variations in bulk density of fluid inclusions. The 2S inclusions are similar to the 2P inclusions in their T_mCO_2 and $T_hCO_2(L)$ values (Fig. 10), which suggests that the 2P and 2S fluid inclusions are similar in composition.

GH-SU-QV-2

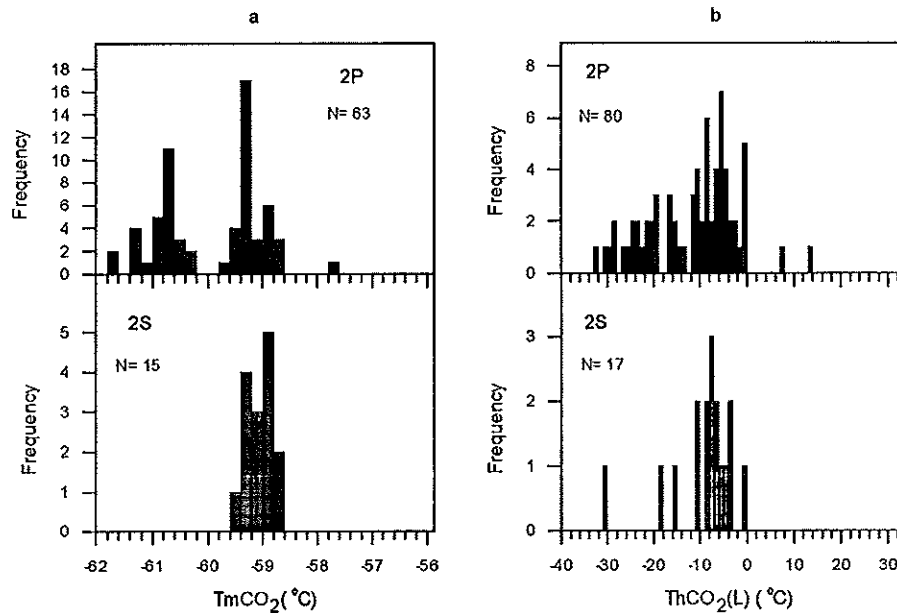


Figure 10. Frequency- $T_m\text{CO}_2$ and - ThCO_2 histograms of 2P and 2S fluid inclusions in vein quartz from the Sansu mine at Ashanti in Ghana. Abbreviations as in Fig. 5.

GH-PT-QV-1

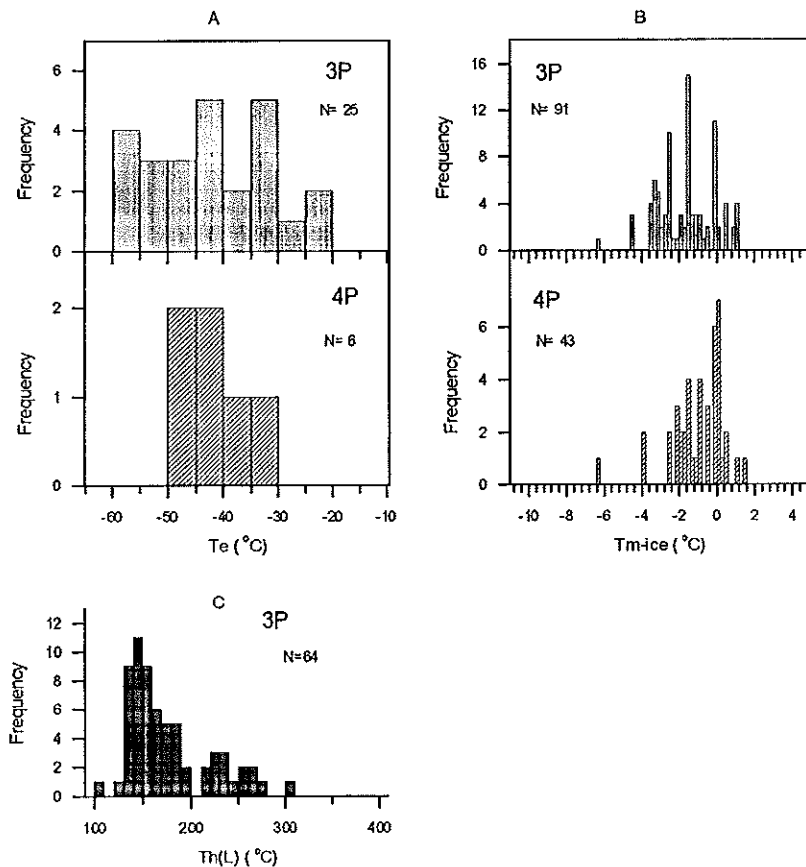


Figure 11. Frequency- T_e and - Tm-ice histograms of 3P and 4P fluid inclusions in vein quartz from the non-mineralized granodiorite at Princess Town in Ghana. T_e =eutectic temperature. Abbreviations as in Fig. 5.

Barren quartz veins from the Princess Town granodiorite: Fluid inclusion populations from the barren quartz veins consist of aqueous, moderate salinity types 3 and 4 only, with no gas-rich types. Secondary 3S inclusions were not measured microthermometrically. Eutectic temperatures (T_e) of 3P inclusions range from -58.6 to -21.4 °C (Fig. 11a), indicating the presence of Na^+ , Ca^{2+} and Mg^{2+} cations in the inclusion fluid. Final melting temperatures of ice ($T_{m\text{-ice}}$) are between -6.3 and +1.2 °C (Fig. 11b), corresponding to salinities from 0 to 9.6 wt.% NaCl equivalent. The positive $T_{m\text{-ice}}$ values were suggested to represent metastable ice without gas bubbles (Roedder, 1984), and their values were not used to estimate salinities of corresponding fluid inclusions. Bulk densities (ρ_b) of the inclusions cluster at 0.99 to 1.06 g/cm³ at 40 °C (Table 5). Total homogenization temperatures of the inclusions range from 108 to 308 °C, with an average value of 176 ± 44 °C (1σ , $n=64$; Fig. 11C). The T_e and $T_{m\text{-ice}}$ values of 4P fluid inclusions are similar to those of the 3P fluid inclusions (Fig. 11A, B), indicating that both 3P and 4P fluid inclusions may have been trapped from an aqueous $\text{H}_2\text{O} \pm \text{NaCl}$ fluid.

Raman microspectrometric results

Gaseous compositions of 88 selected 1P (1P-a, 1P-b), and 2P fluid inclusions from the granitoid-hosted gold deposits were analyzed by Raman microspectrometer and plotted in Fig. 12. With a few exceptions, the Raman-determined compositions of the 1P and 2P fluid inclusions are similar and mainly composed of CO₂ (commonly 80 to 95 mol%), with significant amounts of N₂ (2 to 20 mol%) and CH₄ (0 to 10 mol%). The values of the parameter $100 * \text{CH}_4 / (\text{CH}_4 + \text{CO}_2)$ from the 1P and 2P fluid inclusions mostly fall in a narrow range from 0 to 8% (Fig. 13). As shown in Figure 13, CH₄ contents of fluid inclusions are approximately constant in individual deposits, but show slight variations from one area to another. For example, X_{CH4} values range from 0.011 to 0.022 at Abore North, from 0.002 to 0.004 at Obuasi, and from 0.0 to 0.0001 at Mporhor. The variations of CH₄ in fluid inclusions are probably related to variable oxygen fugacity from one deposit to another (see below).

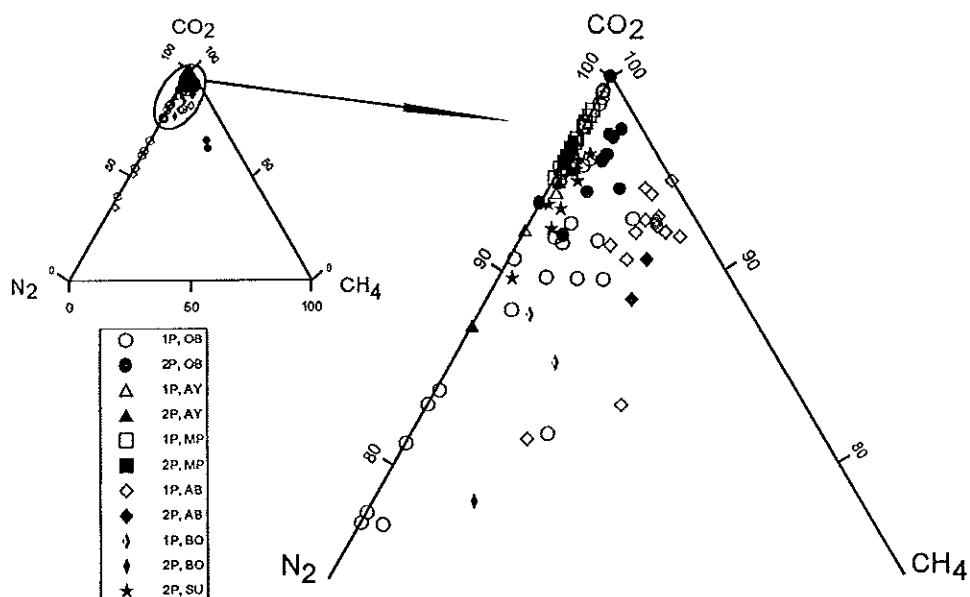


Figure 12. Ternary diagrams showing Raman analyzed gaseous compositions of selected 1P and 2P fluid inclusions from the granitoid-hosted gold deposits and the Sansu mine in Ghana. Abbreviations as in Fig. 5.

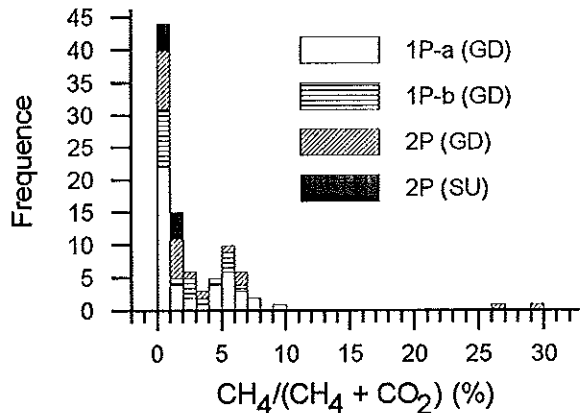


Figure 13. Frequency- $\text{CH}_4/(\text{CH}_4 + \text{CO}_2)$ diagram showing CH_4 distribution for 1P and 2P fluid inclusions from granitoid-hosted gold deposits and for 2P fluid inclusions from the Sansu mine in the Birimian of Ghana.

Raman analyses of 8 selected 2P fluid inclusions from the Sansu mine show that gaseous compositions of the inclusions are dominated by CO_2 (90 to 96 mol%), with minor amounts of N_2 (3 to 10 mol%) and very minor CH_4 (0 to 1 mol%; Fig. 12). Estimated densities of the 2P fluid inclusions typically range from 0.83 to 0.96 g/cm^3 (Table 5). It is evident that the gaseous compositions from the granitoid-hosted gold deposits are comparable with those from the Sansu mine (Fig. 12).

DISCUSSION

Fluid immiscibility

It has been suggested that fluid immiscibility is a common phenomenon associated with gold deposition in a variety of mesothermal and epithermal lode gold deposits from Archean to Tertiary in age (Ho, 1987; Robert and Kelly, 1987; Naden and Shepherd, 1989; Diamond, 1990; Seward, 1991; Bowers, 1991; Craw et al., 1993; Huizenga, 1995; Shimizu et al., 1998; Scott and Watanabe, 1998). On the basis of fluid inclusion data and relative phase proportions, Ramboz et al. (1982) outlined four general criteria for the identification of fluid immiscibility. These are: (1) contemporaneous trapping of two different fluid types reflected in fluid inclusion characteristics; (2) contrasting total homogenization into both the liquid ($T_h(L)$) and vapor ($T_h(V)$) phases over the same range of temperature; (3) the same entrapment pressure at the homogenization temperature of both fluid inclusion types (i.e. if one inclusion type decrepitates before homogenizing, the other type must behave similarly); and (4) compositional constraints (i.e. the distribution coefficient of component i between the fluid (L) and vapor (V) phases ($K_{D,i}^{LV} = X_i^V / X_i^L$) is constant at any specified temperature, pressure, and bulk compositions. Thus, the relevance of the measured values of K_D for components should be systematically checked at the P - T conditions of entrapment. The values of K_D can be compared with their equilibrium distribution coefficients available.

The characteristics of type 1 and type 2 fluids in the present study meet most of the above criteria, and accordingly it is suggested that the H_2O -rich liquid (1P-a) and CO_2 -rich vapor (1P-b, 2P) fluid inclusions represent entrapment of immiscible fluids derived from an

originally homogeneous, one-phase, low-salinity (<6 wt.% NaCl equivalent) H₂O-CO₂ fluid. The observations which support fluid immiscibility in the present study include: (1) the co-existence of different compositional types of 1P-a, 1P-b, and 2P fluid inclusions in close proximity within inclusion arrays from the same quartz grains; (2) a wide range of mole fractions of CO₂ (X_{CO_2} : 0.005 to 0.87), estimated from CO₂ volume proportions at 25 °C, which suggests that these fluid inclusion types were simultaneously trapped; (3) the 1P-a and 1P-b fluid inclusions homogenized either to the aqueous liquid ($T_h(L)$): mainly 200 to 350 °C) or to a homogeneous gaseous phase ($T_h(V)$: dominantly 210 to 350 °C) phases over similar temperature ranges, and the two types of fluid inclusions also decrepitated within the same temperature ranges; (4): variations of CO₂ densities (ρ_c : 0.05 to 1.12 g/cm³) and bulk fluid densities (ρ_b : 0.23 to 1.11 g/cm³) are also consistent with entrapment of two distinctly immiscible fluids; and (5): at room temperature, the 2P fluid inclusions show no visible H₂O phase, but they may contain up to 15 vol% H₂O, as discussed, for example, by Hollister (1990), indicating that they could, therefore, represent an unmixed CO₂-rich and H₂O-poor end-member.

Fluid inclusions in vein quartz from the Yamensakrom prospect and the Sakpa mine are dominantly composed of the 1P-a type. This observation is not consistent with fluid immiscibility. However, the similar geological setting (brittle regime) and deposit characteristics (ore and alteration mineral assemblages) indicate that all the granitoid-hosted gold deposits in the present study underwent a similar process of mineralization. The paucity of other fluid inclusion types (i.e. 1P-b, 2P) at Yamensakrom and Sakpa may, therefore, reflect a sampling bias in the data set, or variations of hydrostatic pressure within fractures, as discussed, for example, by Trumbull et al. (1996). On the other hand, the dominance of H₂O-CO₂±NaCl fluid inclusions at both Yamensakrom and Sakpa may indicate that in certain areas entrapment of the initial homogeneous fluids had taken place prior to fluid immiscibility.

P-T conditions of mineralization

If, as suggested above, the dominant fluid types in the mineralized portions of the Birimian of Ghana were the result of fluid immiscibility, then the homogenization temperatures of the 1P-a and 1P-b fluid inclusions are equivalent to the temperatures of entrapment of inclusion fluids, and they also represent the temperatures of mineralization (e.g., Roedder, 1984). As shown in Figs. 5d, h; Fig. 7b and Tables 2-4, the total homogenization temperatures of 1P and 3P fluid inclusions from individual samples over the entire study area show a large range from about 150 to 380 °C and 160 to 320 °C, respectively, with a mean of 298 ± 48 °C (1σ , n=310) for the 1P and 316 ± 46 °C (1σ , n=69) for the 1P-b. The large variation in homogenization temperatures may result from: (1): the dataset includes all the measured T_h values for individual inclusion types from the entire study area, and is, therefore, characterized by a variance that is far greater than that expected for individual deposits; (2) some primary fluid inclusions with low T_h values from the samples may be secondary in origin; and (3) leakage, stretching, and necking down of fluid inclusions after entrapment may have been affected the range of homogenization temperatures. Thus, a major cluster of homogenization temperatures from individual gold deposits was selected to represent mineralization temperatures, which are summarized in Table 6. The mineralization temperatures from individual granitoid-hosted gold deposits are similar and fall in a range from about 200 to 350 °C (Table 6). In the case of the Yamensakrom prospect and the Sakpa mine, the minimum mineralization temperatures are between 200 and 250 °C, and 230 and 270 °C, respectively. These temperatures are comparable with those (200 to 400 °C) estimated from the alteration mineral assemblages, and they also coincide with temperatures of regional greenschist-facies metamorphism (250 to 400 °C; Klemd et al., 1993).

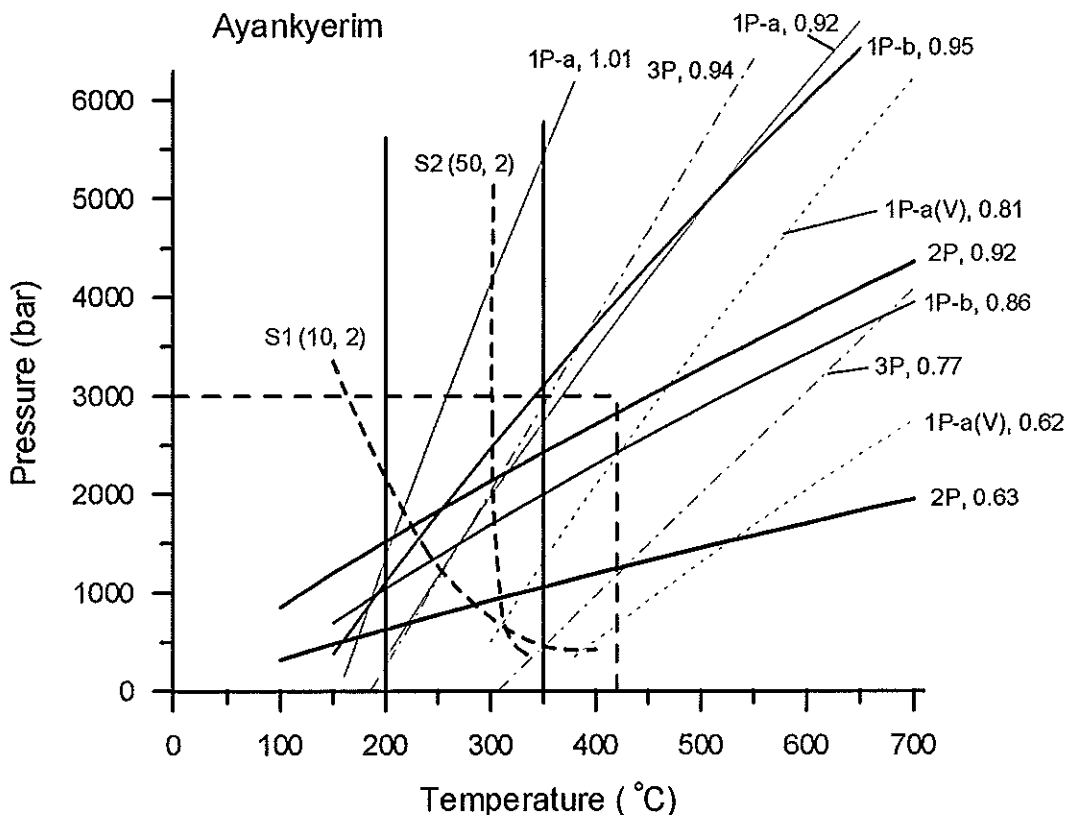


Figure 14. P-T diagram displaying isochores of aqueous H_2O - CO_2 - $NaCl$, H_2O - $NaCl$ and gaseous CO_2 - N_2 - CH_4 fluid inclusions in vein quartz from the Ayankyerim mine at Obuasi. The vertical lines represent temperatures of 200 and 250 °C from the major range of total homogenization temperatures for the 1P and 3P fluid inclusions. The solvi S1 and S2 are defined by average mole % CO_2 and wt. % $NaCl$ of the 1P-a and 1P-b fluid inclusions, respectively, extrapolated from Hagemann and Brown (1996). The maximum P-T limits of regional greenschist facies are from Eisenlohr and Hirdes (1992), Klemd et al. (1993), Klemd and Hirdes (1997). For discussion see text.

Pressures of mineralization were estimated from fluid inclusion P-T isochores that were constructed from the microthermometric data and Raman analyses of fluid inclusions, using published equations of state (see above). The isochor calculations pertain to representative fluid inclusions for each of the major fluid inclusion types. Intersections of inclusion isochores and solvi for the H_2O - CO_2 - $NaCl$ system define the limits of entrapment in both temperature and pressure space (Roedder, 1984; Hagemann and Brown, 1996). Fig. 14 shows a typical example from the Ayankyerim mine at Obuasi. Two vertical lines at 200 and 350 °C represent the common range of trapping temperatures, which are directly obtained from the homogenization temperatures. The solvi S1 (average 10 mole% CO_2 and 2 wt.% $NaCl$ equivalent from the 1P-a inclusions) and S2 (average 50 mole% CO_2 and 2 wt.% $NaCl$ equivalent from the 1P-b inclusions) were extrapolated from Hagemann and Brown (1996). The upper P-T limits of regional greenschist-facies metamorphism were at 420 °C and 3 kbar (Eisenlohr and Hirdes, 1992; Klemd et al., 1993; Klemd and Hirdes, 1997). As shown in Fig. 14, the intersections of isochores and the line of 200 °C give pressures of 0.3 to 1.3 kbar, and the temperature line of 350 °C intersects the isochores at 0.5 to 5.5 kbar. The pressure 5.5 kbar

Table 6. Summary of temperatures and pressures of mineralization for granitoid-hosted gold deposits/prospects from the Birimian of Ghana

Deposit/ prospect	Locality	Belt/ basin	Intruded rock	Tt (°C)	Pt (kbar)	Remark
Mporhor*	Mporhor	Southern Ashanti belt	Meta-volcanics	200 to 370	0.5 to 3	Imm.
Nhyiaso	Obuasi	Southeastern Kumasi basin	Phyllite	200 to 360	0.5 to 3	Imm.
				330 to 380	0.3 to 0.6	$T_hCO_2(V)$
Yamensakrom*	Obuasi	Southeastern Kumasi basin	Phyllite	Min: 200 to 250	Min: 1 to 1.6	
Ayankyerim	Obuasi	Southeastern Kumasi basin	Phyllite	200 to 350	0.3 to 3	Imm.
				300 to 380	0.3 to 0.8	$T_hCO_2(V)$
Chirawewa East	Ayanfuri	Southeastern Kumasi basin	Phyllite	250 to 350	1 to 3	Imm.
Chirawewa West	Ayanfuri	Southeastern Kumasi basin	Phyllite	250 to 350	0.9 to 3	Imm.
				350 to 410	0.4 to 0.6	$T_hCO_2(V)$
Mpesetia	Mpesetia	Northern Asankrangwa belt	Phyllite	220 to 360	0.9 to 3	Imm.
Abore North	Abore	Northern Asankrangwa belt	Phyllite	250 to 340	0.7 to 3	Imm.
Dokrupe	Bole	Southern Bole-Navrongo belt	Phyllite	250 to 360	1.5 to 3	Imm.
Sakpa	Bole	Southern Bole-Navrongo belt	Phyllite	Min: 230 to 270	Min: 1.1 to 1.5	

Note: Tt=Trapping temperature estimated from the major range of microthermometric temperatures of fluid inclusions resolved from fluid immiscibility. Pt=trapping pressures estimated from fluid inclusion isochores. Imm.=fluid immiscibility, Min=minimum. *=prospecting area.

is unreasonably too high considering the brittle structure of mineralization and the greenschist-facies metamorphism. Thus, the mineralization pressures at Ayankyerim are estimated to be between 0.3 and 3 kbar at 200 to 350 °C. For those fluid inclusions, of which the CO₂ part homogenized into the vapor phase, the isochores (1P-a(V)) intersecting the solvus S1 define pressures at 0.3 to 0.8 kbar and temperatures at 300 to 380 °C. The large pressure fluctuations at Ayankyerim may be related to an active fault system during mineralization, such a suggestion has been presented by Hagemann and Brown (1996).

Mineralization pressures for all the other nine granitoid-hosted gold deposits are estimated from fluid inclusion isochores in the same way as discussed above, and these values are shown in Table 6. In all, the mineralization pressures for the 10 gold deposits are similar and commonly fall in the range from 0.3 to 3 kbar. The *P-T* values from the granitoid-hosted gold deposits are consistent with those estimated from the alteration mineral assemblages and the geological setting (brittle structure and greenschist-facies metamorphism), but they are slightly lower than those from the Ashanti- and Tarkwa-type gold deposits (Fig. 15). It is, therefore, suggested that the granitoid-hosted gold deposits in the Birimian of Ghana were formed under mesothermal *P-T* conditions of mineralization, which was related to a late stage of the Birimian orogeny.

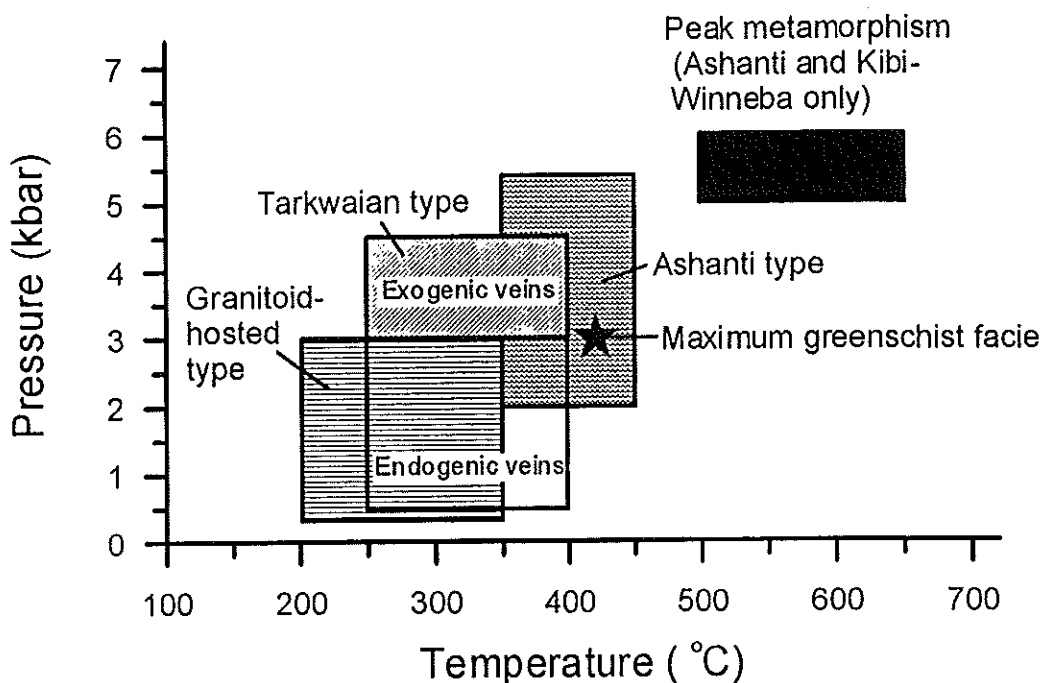


Figure 15. Diagram showing temperature-pressure conditions for peak metamorphism, Ashanti-, Tarkwa-, and granitoid-hosted-type gold deposits from Ghana. Also shown is the maximum P-T point of greenschist facies. Data: Klemd (1998) (peak metamorphism); Schmidt Mumm et al. (1997), Oberthür et al. (1994) (Ashanti type); Klemd et al. (1993) (Tarkwaian type); and Eisenlohr and Hirndes (1992), Klemd et al. (1993), Klemd and Hirndes (1997) (maximum greenschist facies).

In the case of Sansu mine at Ashanti, mineralization P-T conditions were not constructed in the present study. Detailed studies of fluid inclusions from the Ashanti-type gold deposits, especially in the Ashanti region, suggested that the fluid inclusions were modified by grain boundary migration/recrystallization during ductile and brittle transition (e.g., Klemd, 1998). The trapping temperature and pressure of fluid inclusions were estimated to be at 440 °C and 5.4 kbar (Schmidt Mumm et al., 1997), at 400 ± 50 °C and 2 to 4 kbar (Oberthür et al. 1994), and at >420 °C and >3.5 kbar (Schwartz et al., 1992). These results indicate that the Ashanti-type gold deposits, including the Sansu mine, were formed at relatively high temperatures and pressures (i.e. 400 ± 50 °C, 2 to 5.4 kbar).

Oxygen fugacity ($f\text{O}_2$) of ore-forming fluids

If it is suggested that the following equilibrium reaction pertains to the ore fluids in the present study:



then the oxygen fugacity of the fluids can be calculated as:

$\log f\text{O}_2 = 0.5 * (\log f\text{CO}_2 + 2\log f\text{H}_2\text{O} - \log f\text{CH}_4 - \log K_4)$ (for temperatures of 200 to 350 °C and where $\log K=88.2$ at 200 °C and 67.0 at 350 °C; Ohmoto and Kerrick, 1977). This relationship provides lower limits of $f\text{O}_2$ for the ore-bearing hydrothermal fluids in the deposits (Mikuchi and Ridley, 1993).

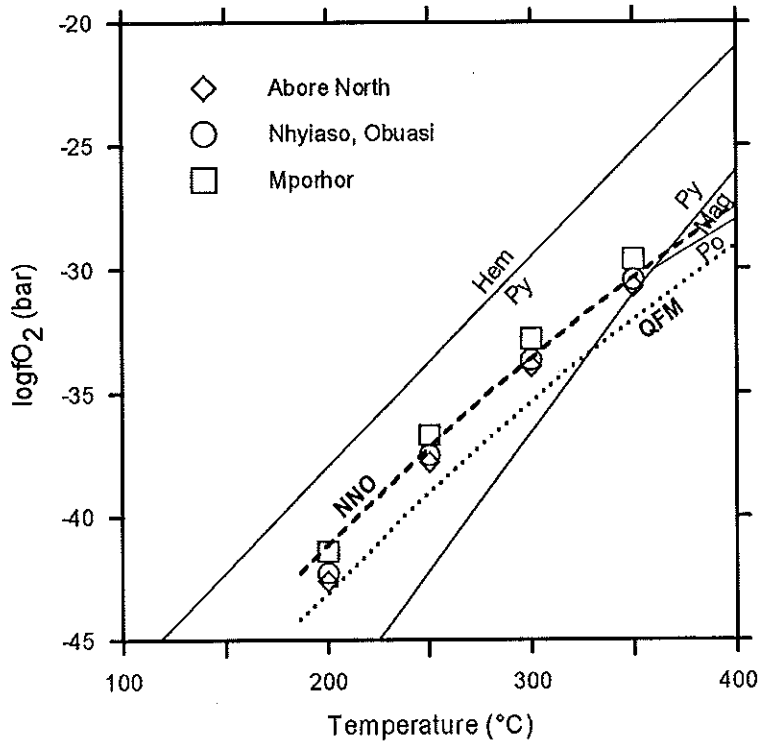


Figure 16. $\log fO_2$ -temperature plot showing oxygen fugacities of mineralizing fluids from Abore North, Nhyiaso, Obusai and Mporhor at 200 to 350 °C, estimated from CO_2 - CH_4 equilibrium. The QFM and NNO buffer curves below 300 °C were extrapolated from Nwe and Morteani (1993). Equilibrium constants are from Ohmoto and Kerrich (1977), and fugacity coefficients of H_2O , CO_2 , and CH_4 at 2000 bar are from Huizenga (1995). Mineral phase boundary lines are from McCuaig and Kerrich (1994). Py=pyrite, Hem=hematite, Po=pyrrhotite, Mag=magnetite.

The average mole fractions of H_2O , CO_2 and CH_4 (X_{H_2O} , X_{CO_2} , X_{CH_4}) were estimated to be 0.7500, 0.2075, and 0.020 at Abore North, 0.8119, 0.1618, and 0.0039 at Nhyiaso, Obusai, and 0.7311, 0.2493, and 0.0001 at Mporhor. The fugacity coefficients of H_2O , CO_2 , CH_4 were calculated from the program of Huizenga (1995) at 2 kbar. The fO_2 values estimated from the above equation at 200 to 350 °C range between $10^{-42.6}$ and $10^{-30.7}$ for the Abore North prospect, $10^{-42.3}$ and $10^{-30.4}$ for the Nhyiaso open pit, and between $10^{-41.4}$ and $10^{-29.6}$ for the Mporhor prospect (Fig. 16). These fO_2 values are equivalent to a range from QFM + 0.5 to QFM + 1.7 and approach the Ni-NiO buffer with decreasing X_{CH_4} (Fig. 16). The trend of increasing CH_4 contents from Abore North to Mporhor is, therefore, reflected in decreasing fO_2 values. As shown in Fig. 16, the estimated fO_2 values fall within the pyrite field, which is consistent with the observed ore mineral assemblages from the granitoid-hosted gold deposits. The ore-forming fluids were in a relative reduced state during mineralization, and this feature is further supported by the absence of magnetite and hematite in the mineral assemblages.

Comparison of granite-hosted gold deposits with the Ashanti and Tarkwaian types

Table 7 summarizes the geological and geochemical characteristics, as well as radiometric ages of the Ashanti, Tarkwaian, and granitoid-hosted deposit types. Although these deposits are different with respect to host rocks, structural setting and ore mineralogy, it

is apparent that the fluids responsible for this widespread mineralization event are both similar and distinctive, and comprise low-salinity $\text{H}_2\text{O}-\text{CO}_2-\text{N}_2\pm\text{CH}_4$ compositions.

The entrapment temperatures and pressures of ore-forming fluids from the mineralized granitoids reflect mesothermal conditions, coincident with the $P-T$ range of regional greenschist-facies metamorphism, whereas those of the Ashanti-type gold deposits formed under somewhat higher $P-T$ conditions (Fig. 15). It has been suggested that the Ashanti-type mineralization was associated with the regional peak of metamorphism (Oberthür et al., 1994), whereas the mineralization within the Birimian granitoids was related to the waning stages of the same regional metamorphic event. In the Tarkwaian conglomerate-hosted gold deposits, the $P-T$ conditions of entrapment from exogenic and endogenic veins are generally comparable with those of both the Ashanti-type and granitoid-hosted gold deposits (Fig. 15), but the temperatures of entrapment generally overlap those of the latter (Fig. 15). The $P-T$ ranges suggest that the Tarkwaian gold deposits may also have been significantly influenced by the same regional mineralizing fluids that were responsible for the Ashanti-type gold deposits (Klemd et al., 1993; Hirdes and Nunoo, 1994), which is supported by the fact that the ore mineral assemblage in the Tarkwaian deposits is largely of an authigenic nature, reflecting substantial alteration/mineralization by later relatively oxidized fluids.

The present study and previous publications reveal that fluid inclusions in vein quartz from granitoid-hosted-, Ashanti-, and Tarkwa-type gold deposits are distinctly different from barren quartz veins and barren quartz-pebble conglomerates (Schwartz et al., 1992; Klemd et al., 1993; Oberthür et al., 1994; Klemd and Hirdes, 1997; Schmidt Mumm et al., 1997). The results indicate that fluid inclusions are a useful tool for regional gold exploration in the Birimian terrane of Ghana. In mineralized areas, it is to be expected that fluid inclusions will be the $\text{H}_2\text{O}-\text{CO}_2\pm\text{NaCl}$ and/or $\text{CO}_2-\text{N}_2\pm\text{CH}_4$ types (Table 6), whereas in barren areas, fluid inclusions will be dominated by $\text{H}_2\text{O}\pm\text{NaCl}$ composition.

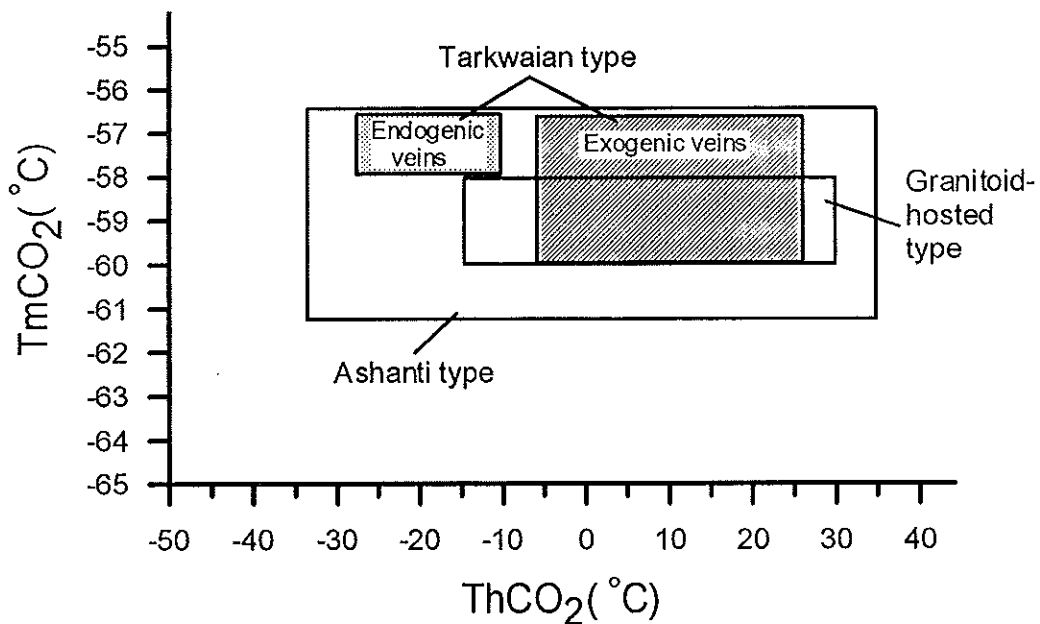


Figure 17. Diagram illustrating $T_m\text{CO}_2$ and $T_h\text{CO}_2$ ranges for 2P fluid inclusions from the Ashanti-, Tarkwa-, and granitoid-hosted-type gold deposits in the Birimian of Ghana. Data: Oberthür et al. (1994) (Ashanti type); Klemd et al. (1993) (Tarkwaian type); and this study (granitoid-hosted type).

Table 7. Summary of geological and geochemical characteristics for the Ashanti, Tarkwaian, and granitoid-hosted types of gold deposits from the Birimian of Ghana

Item	Granitoid-hosted type	Ashanti type	Tarkwaian type
Occurrence	Volcanic belt and sedimentary basin	Volcanic belt	Volcanic belt
Host rock	Granitoids (tonalite, granodiorite to granite)	Meta-volcanics, meta-sediments	Conglomerates
Intruded or country rock	Meta-volcanics in belt, phyllite in basin or belt	Meta-volcanics, meta-sediments	Conglomerates, sandstones, phyllites, schists, grits
Structure	Major NE-striking faults	NE-striking shear zones	NE-striking faults
Mineralization type	Quartz veins and veinlets, pervasive alteration zones	Disseminated sulfides and quartz veins	Palaeo-placer
Ore mineral	Py, Asp, Cp, Sph, Ht, Au	Asp, Py, Po, Mc, Cp, Sph, Gal, Bn, Tet, Au	Heavy mineral: Ht, Mt, Im, Au; authigenic mineral: Py, Cp, Bn, Po, Au
Ore geochemistry	Fe-As-S-Au	Fe-As-S-Au, Pb-Sb-Cu-Zn-S-Au-Ag	Fe-Ti-Au
Wall rock alteration	Py, Asp, Sil, Ser, Mus, Chl, Tou, Carb	Carb, Asp, Py, Mus, Kao	Weak sulfidization (mainly Py)
Alteration geochemistry	Enriched elements: CO ₂ , N ₂ , CH ₄ , S, As, Au	Enriched elements: CO ₂ , N ₂ , CH ₄ , S, As, Pb, Zn, Cu, Ag, Au,	Weakly enriched elements: S, Cu, Pb, Cu, Au
Fluid inclusions	H ₂ O-CO ₂ ±NaCl, CO ₂ -N ₂ ±CH ₄ , H ₂ O±NaCl (<10%)	CO ₂ -N ₂ ±CH ₄ (>90%), H ₂ O-CO ₂ ±NaCl (up to 5%), H ₂ O-NaCl (5 to 10%)	CO ₂ -N ₂ ±CH ₄ (85%), H ₂ O-CO ₂ ±NaCl (5%), H ₂ O-NaCl (10%)
Salinity (wt.% NaCl equivalent)	Commonly 0 to 6, locally up to 13	0 to 5 (6), 2 to 11, up to 25 (8)	0 to 12
Tfi (°C)	160 to 380 (commonly 220 to 350)	215 to 405 (6), 128 to 280 (8)	140 to 380 °C (aqueous inclusions)
Tmin (°C)		Max: 370 to 470 at 2 kbar (6)	
Tt (°C)	200 to 380 (commonly 200 to 350)	220 to 440 (8) 280 to 450 (2)	250 to 400 °C
Pt (kbar)	0.3 to 3	1.9 to 5.4 (8) 2 to 4 (2)	0.5 to 3 kbar (endogenic veins), 3 to 4.5 kbar (exogenic veins)
Mineralization age	2086 ± 4 to 2098 ± 7 (U-Pb rutile from Basin granitoids) (3), 2110 ± 32 to 2133 ± 21 (U-Pb rutile from Belt granitoids) (1)	2116 ± 2 to 2132 ± 3 (U-Pb zircon) (2), 1940 to 2122 (Pb-Pb Gal-Bn model age) (9) 2039 to 2107 (Pb-Pb gold grain model age) (9)	2095 ± 10 to 2132 ± 3 Ma (U-Pb zircon)
Genesis	Late-metamorphic (1)	Syn-metamorphic (2)	Palaeo-placer (12)
Ref.	1, 3, 4	2, 3, 4, 5, 6, 7, 8, 9	10, 11, 12

Note: Py=pyrite, Asp=arsenopyrite, Au=native gold, Bn=bournonite, Carb=carbonate, Chl=chlorite, Cp=chalcopyrite, Gal=galena, Ht=hematite, Im=ilmenite, Kao=kaolinite, Mc=marcasite, Mt=magnetite, Mus=muscovite, Po=pyrrhotite, Ser=sericite, Sil=silica, Sph=sphalerite, Tet=tetrahedrite, Tou=tourmaline. Tmin=temperature estimated from mineral equilibrium, Tfi=temperature from fluid inclusion microthermometry, Tt=trapped temperature from inclusion microthermometric data, Pt=trapped isochorral pressure. Number in parentheses refers to the reference. Ref.: 1: this study; 2: Oberthür et al. (1994); 3: Oberthür et al. (1996); 4: Oberthür et al. (1998); 5: Hirdes and Leube (1989); 6: Schwartz et al. (1992); 7: Klemd and Hirdes (1997); 8: Schmidt Mumm et al. (1997); 9: Höhndorf et al. (1994); 10: Milési et al. (1991); 11: Klemd et al. (1993); 12, Hirdes and Nunoo (1994).

The fluid inclusion data obtained in the present study indicate that ore-forming fluids from the major granitoid-hosted gold deposits in the Birimian terrane of Ghana were originally homogeneous $\text{H}_2\text{O}-\text{CO}_2\pm\text{NaCl}$ fluids, containing minor $\text{N}_2\pm\text{CH}_4$. The fluids are characterized by low salinities of commonly less than 6 wt.% NaCl equivalent and underwent phase separation at about 200 to 350 °C and 0.3 to 3 kbar. Because of fluid immiscibility, original compositions of the fluids cannot be estimated from the fluid inclusions alone. The gaseous compositions and salinities of ore-forming fluids from the granitoid-hosted gold deposits are comparable with those from the Ashanti- and Tarkwaian-type gold deposits (Fig. 17, Table 7). These diagnostic fluid characteristics suggest a genetic link between the mineralizing fluids among all three gold deposit types in Ghana. The alteration and ore mineral assemblages indicate that the ore-forming fluids were reduced (\log/O_2 above QFM) at near neutral pH values (about 5 to 6) during mineralization within the above *P-T* conditions.

Sources of ore-forming fluids

The fluid characteristics of granitoid-hosted gold deposits are also comparable with those of mesothermal lode gold deposits in Archean greenstone terranes elsewhere in the world, in which the ore-forming fluids are low-salinity (typically <6 wt.% NaCl equivalent) $\text{H}_2\text{O}-\text{CO}_2$ -rich fluids, with minor N_2 and/or CH_4 compositions, with mineralization forming at 300 ± 50 °C and 1 to 3 kbar in ductile to brittle structures (Ho, 1987; Groves and Foster, 1991; De Ronde et al., 1992; McCuaig and Kerrich, 1994; Solomon and Groves, 1994; Huizenga, 1995; Hagemann and Brown, 1996; Cassidy et al., 1998). The prevailing view is that the fluids in many Archean mesothermal gold deposits were metamorphic in origin.

This metamorphic model appears to be valid for the present study. The following points support the proposition that gold mineralization in the Birimian terrane of Ghana is related to circulation of a regional metamorphic fluid: (1) the major ore sulfides (mainly pyrite and arsenopyrite) from the granitoid-hosted gold deposits are the same as the Ashanti-type gold deposits, and fluid inclusions are similar in composition for both gold deposit types, suggesting a genetic link between the two types of gold deposits; (2) the low-salinity, CO_2 -rich fluids reflect a metamorphic process involving devolatilization of the Birimian rocks (see below), but exclude the possibility of magmatic fluids as a source; (3) The *P-T* conditions of ore formation coincide with those of the regional greenschist-facies metamorphism present in the area, but are lower than those of the peak metamorphism (epidote-amphibole and amphibole facies; Fig. 15), indicating that mineralization in the granitoids occurred at a late stage of regional metamorphism; (4) U-Pb zircon and rutile isotopic dating reveals that the mineralization is significantly younger, by 5 to 30 million years, than the ages of the corresponding granitoid intrusion (Oberthür et al., 1998; Yao and Robb, 1999).

Metamorphism and gold mineralization

Regional metamorphism in the Birimian of Ghana was related to the Eburnean tectonothermal event (Leube and Hirdes, 1986; Hirdes and Leube, 1989; Eisenlohr and Hirdes, 1992, Oberthür et al., 1998). The metamorphic grade of Birimian rocks is typically greenschist facies and the general lack of biotite indicates that the peak metamorphic temperature was <420 °C (Eisenlohr and Hirdes, 1992). However, in parts of the Ashanti and Kibi Winneba belts, metamorphic grades reached the epidote-amphibolite and amphibolite facies, indicating peak metamorphic conditions of 500 to 650 °C and 5 to 6 kbar (Klemd, 1998), which are comparable with upper *P-T* estimates from entrapment temperatures and pressures of fluid inclusions for the Ashanti mine. These *P-T* conditions are higher than the maximum estimates

obtained for the granitoid-hosted gold deposits, which are about 350 °C and 3 kbar (Fig. 15).

On the basis of stable isotope geochemistry of ores from the Ashanti mine, Oberthür et al. (1996) suggested that the mineralizing fluids had interacted with deep-seated Birimian rocks (mainly sedimentary rocks), and that the metamorphic fluids were derived from devolatilization reactions within Birimian strata during prograde metamorphism. This proposal is consistent with the fluid inclusion data and explains:

(1) the high CO₂ and CH₄ contents in the fluid, which accords with the fact that Birimian rocks contain significant amounts of carbonaceous matter (0.4 to 5.2 wt%, n=28, Oberthür et al., 1996) and could provide CO₂ and CH₄ to a fluid phase generated during prograde metamorphism; and

(2) the N₂ component in the fluids, which may have been derived from biologically fixed nitrogen in metasedimentary rocks or from release of NH⁺-ions in pre-metamorphic minerals (feldspar, amphibole, sheet silicates) within the rocks that were subjected to metamorphism (Andersen et al., 1989; Meyer and Ridgway, 1991). On the basis of ammonium analyses for samples from the Kimberley Reef, Meyer and Ridgway (1991) suggested that the ammonium in Witwatersrand rocks may indicate their metamorphic origin. It is speculated that significant amounts of N₂ were probably related to amphibolite-granulite facies metamorphism at depth, since the N₂ contents from both the granitoid-hosted and Ashanti-type gold deposits are similar. The deep-seated N₂ ascended to high levels along crustal-scale faults and shears, such as the Ashanti shear zones, and was incorporated into the mineralizing fluids associated with a range of metamorphogenic gold deposits.

A detailed discussion on gold transportation and deposition is beyond the scope of this study. Based on the fluid inclusion data and ore geochemistry, however, it is suggested that gold-thio-complexes were the major species in the ore-forming fluids (Seward, 1991; Shenberger and Barnes, 1989; Hayashi and Ohmoto, 1991) and gold deposition from the fluids may have resulted from fluid phase separation and/or sulphidization of wall rocks. Variations in *fO*₂ are not considered to be a significant factor for gold deposition because constant CH₄ contents in fluids from individual gold deposits suggest static local *fO*₂ conditions during mineralization.

CONCLUSIONS

Fluid inclusions in vein quartz from ten granitoid-hosted gold deposits and prospects in the Birimian terrane of Ghana are dominantly composed of aqueous H₂O-CO₂±NaCl and gaseous CO₂-N₂±CH₄ types, with minor (<10%) aqueous H₂O±NaCl types. The range of fluid compositions, as indicated by CO₂ volume proportions in fluid inclusions, and similar total homogenization temperature ranges (Th(L): commonly 200 to 350 °C; Th(V): typically 210 to 350 °C) suggest that the inclusions were trapped from fluid immiscibility. Salinities of inclusion fluids are commonly between 0 and 6 wt.% NaCl equivalent, and total densities of inclusions typically range from 0.65 to 0.95 g/cm³. The microthermometry-based temperature and pressure estimates of trapped inclusion fluids are between 200 and 350 °C, and 0.3 and 3 kbar. These values agree with the mesothermal *P-T* conditions estimated from the alteration and ore mineral assemblages, and they are also consistent with the *P-T* conditions of regional greenschist-facies metamorphism. Raman analyses show that the gaseous component of fluid inclusions is mainly composed of CO₂ (80 to 95 mol%), with significant amounts of N₂ (2 to 20 mol%) and minor CH₄ (0 to 10 mol%).

The low-salinity H₂O-CO₂-rich fluids are consistent with metamorphic derivation and were probably developed during the regional deformation and metamorphism of the Eburnean orogeny. Gold deposition from the fluids is suggested to result from phase separation and

sulphidization of wall rocks. No specific granitoid type is related to gold mineralization, and the granitoids merely acted as preferential conduits for fluid flow. The fluid inclusion data, the geological setting, the ore geochemistry, and the U-Pb isotopic dating, suggest that the granitoid-hosted and Ashanti-type lode gold deposits in the Birimian terrane of Ghana represent a continuum of processes of mineralization spanning syn- to late-stage metamorphism during the Eburnean orogeny.

ACKNOWLEDGEMENTS

This paper forms part of a post-doctoral project by the first author, for which financial support by Gold Fields of South Africa (now Gold Fields Ltd.: GFL) and FRD-THRIP is gratefully acknowledged. R. P. Viljoen (University of the Witwatersrand), R. Lipson and J. Misiewicz (GFL), M. J. Botha, B. Nunoo and H. A. MacLaren (Gold Fields Ghana Ltd.) are thanked for assistance and support during the project work. R. Mauer kindly permitted access to unpublished data from his PhD thesis. G. Loh (Ghana Geological Survey Accra), Y. Iddirisu and T. Akabzaa (University of Ghana, Legon) are thanked for the provision of additional information. C. Penner and P. Gibbon (Mutual Ghana Ltd.) permitted access to the Mpesisita and Abore North prospects. J. A. Amanor, C. Asamoah-Owusu, S. M. Bosomtwe and Y. A. Acheampong (Ashanti Goldfields Co.) helped with access to the Obuasi and Ayanfuri open pits and to the Ashanti mine. K. Atta-Ntim (Kumasi Geological Survey) collaborated in field trips in the Kumasi area. A. Fosu (Takoradi Gold N.L.) helped with access to the Bole mine. Finally, we are grateful to three Economic Geology reviewers for their constructive and incisive comments, which substantially improved the presentation of this paper.

REFERENCES

- Andersen, T., Burke, E. A. J. and Austrheim, H., 1989, Nitrogen-bearing, aqueous fluid inclusions in some eclogites from the Western Gneiss Region of the Norwegian Caledonides. *Contrib. Mineral. Petrol.*, v. 103, p. 153-165.
- Bowers, T. C. and Helgeson, H. C., 1983, Calculation of the thermodynamic and geochemical consequences of nonideal mixing in the system H_2O-CO_2-NaCl on phase relations in geologic system: Equation of state for H_2O-CO_2-NaCl fluids at high pressures and temperatures. *Geochim. Cosmochim. Acta*, v. 47, p. 1247-1275.
- Bowers, T. S., 1991, The deposition of gold and other metals: Pressure-induced fluid immiscibility and associated stable isotope signatures. *Geochim. Cosmochim. Acta*, v. 55, p. 2417-2434.
- Cassidy, K. F., Groves, D. I. and McNaughton, N. J., 1998, Late-Archean granitoid-hosted lode-gold deposits, Yilgarn Craton, Western Australia: Deposit characteristics, crustal architecture and implications for ore genesis. *Ore Geol. Rev.*, v. 13, p. 65-102.
- Craw, D., Teagle, D. A. H. and Belocky, R., 1993, Fluid immiscibility in late-Alpine gold-bearing veins, Eastern and Northwestern European Alps. *Mineral. Deposita*, v. 28, p. 28-36.
- Davis, D.W., Hirdes, W., Schaltegger, E. and Nunoo, E. A., 1994, U/Pb age constraints on deposition and provenance of Birimian and gold-bearing sediments in Ghana, West Africa. *Precam. Res.*, v. 67, p. 89-107.
- De Ronde, C. E. J., Spooner, E. T. C., De Wit, M. J. and Bray, C., 1992, Shear zone-related, Au quartz vein deposits in the Barberton greenstone belt, South Africa: Field and petrographic characteristics, fluid inclusion properties, and light stable isotope geochemistry. *Econ. Geol.*, v. 87, p. 366-402.
- Diamond, L. W., 1990, Fluid inclusion evidence for P-V-T-X evolution of hydrothermal solutions in Late-Alpine gold-quartz veins at Brusson, Val D'Ayas, Northwest Italian Alps. *Am. J. Sci.*, v. 290, p. 912-958.
- Diamond, L. W., 1994, Salinity of multivolatile fluid inclusions determined from clathrate hydrate stability. *Geochim. Cosmochim. Acta*, v. 58, p. 19-41.
- Eisenlohr, B. N. and Hirdes, W., 1992, The structural development of the Early Proterozoic Birimian and Tarkwaian rocks of southwest Ghana, West Africa. *Jour. Afr. Earth Sciences*, v. 14, p. 313-325.
- Groves, D. I. and Foster, R. P., 1991, Archean lode gold deposits. In: Foster, R. P. (ed.) *Gold Metallogeny and Exploration*. Blackie, London, p. 63-103.
- Hagemann, S. G. and Brown, P. E., 1996, Geobarometry in Archean lode-gold deposits. *Eur. J. Mineral.*, v. 8, p. 937-960.
- Hall, D. L. and Bodnar, R. J., 1990, Methane in fluid inclusions from granulites: a product of hydrogen diffusion? *Geochim. Cosmochim. Acta*, v. 54, p. 641-651.
- Hayashi, K. I. and Ohmoto, H., 1991, Solubility of gold in NaCl- and H_2S -bearing aqueous solutions at 250-350 °C. *Geochim. Cosmochim. Acta*, v. 55, p. 2111-2126.
- Hirdes, W. and Leube, A., 1989, On gold mineralization of the Proterozoic Birimian Supergroup in Ghana/West Africa. *Bundesanstalt für Geowissenschaften und Rohstoffe*, Hannover, 179 p.
- Hirdes, W. and Nunoo, B., 1994, The Proterozoic Paleoplacers at Tarkwa gold mine, SW Ghana: Sedimentology, mineralogy, and precise age dating of the Main Reef and West Reef, and bearing of the investigations on source area aspects. In: Oberthür, T. (ed.) *Metallogenesis of selected gold deposits in Africa*. *Geol. Jb.* D100, p. 247-311.

- Hirdes, W., Davis, D. W. and Eisenlohr, B. N., 1992, Reassessment of Proterozoic granitoid ages in Ghana on the basis of U/Pb zircon and monazite dating. *Precam.Res.*, v.56, p. 89-96.
- Hirdes, W., Senger, R., Adjei, J., Efa, E., Loh, G. and Tettey, A., 1993, Explanatory notes for the geological map of southwest Ghana 1:100,000. E. Schweizerbart'sche Verlagsbuchhandlung, Stuttgart, Hannover, 139 p.
- Hollister, L. S., 1990, Enrichment of CO₂ in fluid inclusions in quartz by removal of H₂O during crystal-plastic deformation. *J. Struct. Geol.*, v. 12, p. 895-901.
- Ho, S. E., 1987, Fluid inclusions: Their potential as an exploration tool for Archaean gold deposits. In: Ho, S. E. and Groves, D. I. (eds.) Recent advances in understanding Precambrian gold deposits. I. Univ. West. Aust. Geol. Dept. & Univ. Exten. Publ., 11, p. 239-263.
- Höhndorf, A., Oberthür, T., Gast, L., Vetter, U. and Schmidt Mumm, A., 1994, Lead isotope systematics of the mineralization at the Ashanti gold mine, Obuasi, Ghana. In: Oberthür, T. (ed.) Metallogenesis of selected gold deposits in Africa. *Geol. Jb.* D100, p. 155-165.
- Holloway, J. R., 1981, Compositions and volumes of supercritical fluids in the earth's crust. In: Hollister, L. S. and Carwford, M. L. (eds.) MAC Short course in Fluid Inclusions. *Mineral. Assoc. Can.* 6, p. 13-88.
- Huizenga, J. M., 1995, Fluid evolution in shear zones from the Late Archean Harare-Shamva-Bindura Greenstone Belt (NE Zimbabwe): Thermodynamic calculations of the C-O-H system applied to fluid inclusions. *Netherlands Research School of Sedimentary Geology* Publ., 146 p.
- Junner, N. R., 1940, Geology of the Gold Coast and Western Togoland. *Bull. Gold Coast Geol. Surv.*, v. 11, 40 p.
- Klemd, R. and Hirdes, W., 1997, Origin of an unusual fluid composition in Early Proterozoic palaeoplacer and lode-gold deposits in Birimian greenstone terranes of West Africa. *S. Afr. J. Geol.*, v. 100 (4), p. 405-414.
- Klemd, R., 1998, Comment on the paper by Schmidt Mumm et al. High CO₂ content of fluid inclusions in gold mineralizations in the Ashanti Belt, Ghana: a new category of ore forming fluids? (*Mineral. Deposita* 32: 107-118, 1997). *Mineral. Deposita*, v. 33, p. 317-319.
- Klemd, R., Hirdes, W., Olesch, M. and Oberthür, T., 1993, Fluid inclusions in quartz-pebbles of the gold-bearing Tarkwaian conglomerates of Ghana as guides to their provenance area. *Mineral. Deposita*, v. 28, p. 334-343.
- Klemd, R., Hünen, U. and Olesch, M., 1996 Fluid composition and source of Early Proterozoic lode gold deposits of the Birimian volcanic belt, West Africa. *Intern. Geol. Rev.*, v. 38, p. 22-32.
- Leube, A. and Hirdes, W., 1986, The Birimian Supergroup of Ghana: Depositional environment, structural development and conceptual model of an Early Proterozoic suite. Federal Ministry for Economic Cooperation, Hannover, 259 p.
- Leube, A., Hirdes, W., Mauer, R. and Kesse, G. O., 1990, The early Proterozoic Birimian Supergroup of Ghana and some aspects of its associated gold mineralization. *Precam. Res.*, v. 46, p. 139-165.
- Loh, G. and Hirdes, W., 1996, Explanatory notes for the geological map of southwest Ghana 1:100,000 sheets Sekondi (0402A) and Axim (0403B). *Ghana Geol. Surv. Bull.*, 49, 63 p.
- Mauer, R., 1986, Granitoids. In: Leube, A. and Hirdes, W. (eds.) The Birimian Supergroup of Ghana: Depositional environment, structural development and conceptual model of an Early Proterozoic suite. Federal Ministry for Economic Cooperation, Hannover, p. 125-149.
- Mauer, R., 1990, Petrographische und geochemische Untersuchungen der präkambrischen (Birimian) Granitoide Ghanas. Unpubl. Ph. D. thesis, Tech. Univ. Berlin, 202 p.
- McCuag, T. C. and Kerrich, R., 1994, P-T-t-Deformation-fluid characteristics of lode gold deposits: Evidence from alteration systematics. In: Lentz, D. R. (ed.) Alteration and alteration processes associated with ore-forming systems. *Geol. Assoc. Can. Short Course Note*, No. 11, p. 339-379.
- Meyer, F. M. and Ridgway, J., 1991, Ammonium in Witwatersrand reefs: a possible indicator of metamorphic fluid flow. *S. Afr. J. Geol.*, v. 94, p. 343-347.
- Mikucki, E. J. and Ridley, J. R., 1993, The hydrothermal fluid of Archean lode-gold deposits at different metamorphic grades: compositional constraints from ore and wallrock alteration assemblages. *Mineral. Deposita*, v. 28, p. 469-481.
- Milési, J. P., Ledru, P., Ankrah, P., Johan, V., Maxcoux, E. and Vinchon, C., 1991, The metallogenic relationship between Birimian and Tarkwaian gold deposits in Ghana. *Mineral. Deposita*, v. 26, p. 228-238.
- Naden, J. and Shepherd, T. J., 1989, Role of methane and carbon dioxide in gold deposition. *Nature*, v. 342, p. 793-795.
- Nwe, Y. Y. and Morteiani, G., 1993, Fluid evolution in the H₂O-CH₄-CO₂-NaCl system during emerald mineralization at Gravelotte, Murchison greenstone belt, Northeast Transvaal, South Africa. *Geochim. Cosmochim. Acta*, v. 57, p. 89-103.
- Oberthür, T., Schmidt Mumm, A., Vetter, U., Simon, K. and Amanor, J. A., 1996, Gold mineralization in the Ashanti belt of Ghana: Genetic constraints of the stable isotope geochemistry. *Econ. Geol.*, v. 91, p. 289-301.
- Oberthür, T., Vetter, U., Davis, D. W. and Amanor, J. A., 1998, Age constraints on gold mineralization and palaeoproterozoic crustal evolution in the Ashanti belt of southern Ghana. *Precam. Res.*, v. 89, p. 129-143.
- Oberthür, T., Vetter, U., Mumm, A. S., Weiser, T., Amanor, J. A., Gyapong, W. A., Kumi, R. and Blenkinsop, T. G., 1994, The Ashanti gold mine at Obuasi, Ghana: Mineralogical, geochemical, stable isotope and fluid inclusion studies on the metallogenesis of the deposit. In: Oberthür, T. (ed.) Metallogenesis of selected gold deposits in Africa. *Geol. Jb.* D100, p. 31-129.
- Ohmoto, H. and Kerrick, D., 1977, Devolatilization equilibria in graphitic systems. *Am. J. Sci.*, v. 277, p. 1013-1044.
- Ramboz, C., Pichavant, M. and Weisbrod, A., 1982, Fluid immiscibility in natural processes: Use and misuse of fluid inclusion data. II. Interpretation of fluid inclusion data in terms of immiscibility. *Chem. Geology*, v. 37, p. 29-46.
- Robert, F. and Kelly, W. C., 1987, Ore-forming fluids in Archean gold-bearing quartz veins at the Sigma mine, Abitibi greenstone belt, Quebec, Canada. *Econ. Geol.*, v. 82, p. 1464-1482.
- Roedder, E., 1963, Studies of fluid inclusions II: Freezing data and their interpretation. *Econ. Geol.*, v. 58, p. 167-211.
- Roedder, E., 1984, Fluid inclusions. Review in *Mineralogy*, v. 12, Mineral. Soc. Am., BookCrafters, Inc., Chelsea, Michigan, 644 p.
- Rosso, K. M. and Bodnar, R. J., 1995, Microthermometric and Raman spectroscopic detection limits of CO₂ in fluid inclusions and the Raman spectroscopic characterization of CO₂. *Geochim. Cosmochim. Acta*, v. 59, p. 3961-3975.
- Schmidt Mumm, A., Oberthür, T., Vetter, U. and Blenkinsop, T. G., 1998, High CO₂ content of fluid inclusions in gold mineralizations in the Ashanti Belt, Ghana: a new category of ore forming fluids?-a reply. *Mineral. Deposita*, v. 33, p. 320-322.
- Schmidt Mumm, A., Oberthür, T., Vetter, U. and Blenkinsop, T. G., 1997, High CO₂ content of fluid inclusions in gold mineralizations in the Ashanti Belt, Ghana: a new category of ore forming fluids? *Mineral. Deposita*, v. 32, p. 107-118.
- Schwartz, M. O., Oberthür, T., Amanor, J. and Gyapong, W. A., 1992, Fluid inclusion re-equilibration and P-T-X constraints on fluid evolution in the Ashanti gold deposit, Ghana. *Eur. J. Mineral.*, v. 4, p. 1017-1033.
- Scott, A. M. and Watanabe, Y., 1998, "Extreme boiling" model for variable salinity of the Hokko low-sulfidization epithermal Au prospect, southwestern Hokkaido, Japan. *Mineral. Deposita*, v. 33, p. 568-578.
- Seward, T. M., 1991, The hydrothermal geochemistry of gold. In: Foster, R. P. (ed.) *Gold Metallogeny and Exploration*. Blackie, London, p. 37-62.
- Shenberger, D. M. and Barnes, H. L., 1989, Solubility of gold in aqueous solutions from 150 to 350 °C. *Geochim. Cosmochim. Acta*, v. 53, p. 269-278.
- Shimizu, T., Matsueda, H., Ishiyama, D. and Matsubaya, O., 1998, Genesis of epithermal Au-Ag mineralization of the Koryu mine, Hokkaido, Japan. *Econ. Geol.*, v. 93, p. 303-325.

- Solomon, M. and Groves, D. I., 1994, The geology and origin of Australia's mineral deposits. Oxford Sci. Publ., 951 p.
- Taylor, P. N., Moorbatn, S., Leube, A. and Hirdes, W., 1988, Geochronology and crustal evolution of Early Proterozoic granite-greenstone terrains in Ghana/West Africa. Abstr., Intern. Conf. on the Geology of Ghana, with special emphasis on gold. 75th Anniv. of Ghana. Geol. Surv. Depart., Accra, p. 43-45.
- Taylor, P. N., Moorbatn, S., Leube, A. and Hirdes, W., 1992, Early Proterozoic crustal evolution in the Birimian of Ghana: Constraints from geochronology and isotope geochemistry. Precam. Res., v. 56, p. 97-111.
- Thiéry, R., Martinus, V. D. K. and Dubessy, J., 1994, vX properties of CH₄-CO₂ and CO₂-N₂ fluid inclusions: modelling for T <31°C and P <400 bars. Eur. J. Mineral., v. 6, p. 753-771.
- Trumbull, R. B., Liu, H., Lehrberger, G., Satir, M., Wimbauer, T. and Morteani, G., 1996, Granitoid-hosted gold deposits in the Anjiayingzi district of Inner Mongolia, People's Republic of China. Econ. Geol., v. 91, p. 875-895.
- Van den Kerkhof, A. M., 1988, The system CO₂-CH₄-N₂ in fluid inclusions: Theoretical modelling and geological applications. Free University Press, Amsterdam, 207 p.
- Yao, Y. and Robb, L. J., 1998a, A summary of recent field investigations and sampling of granitoids in the Birimian terrain of Ghana (08 September to 19 October, 1997). Interim report to Gold Fields of South Africa Ltd., Univ. of the Witwatersrand, 48 p.
- Yao, Y. and Robb, L. J., 1998b, The Birimian granitoids of Ghana: A review. Economic Geology Research Unit (EGRU), University of the Witwatersrand, Information Circular No.322, 46 p.
- Yao, Y. and Robb, L. J., 1999, Gold mineralization associated with the Birimian granitoids of Ghana. Final report to Gold Fields of South Africa Ltd., Univ. of the Witwatersrand, 247 p.
- Zhang, Y. and Frantz, J. D., 1987, Determination of the homogenization temperatures and densities of supercritical fluids in the system NaCl-KCl-CaCl₂-H₂O using synthetic fluid inclusions. Chem. Geol., v. 64, p. 335-350.

oo